Characterization of Noise in Uncooled IR Bolometer Arrays

by

William Alexander Lentz

S. B., Massachusetts Institute of Technology (1997)

Submitted to the
Department of Electrical Engineering and Computer Science
in partial fulfillment of the requirements for the degree of

Master of Engineering in Electrical Engineering and Computer Science

at the

MASSACHUSETTS INSTITUTE OF TECHNOLOGY

May 1998
[June 1998]

Author .....
Department of Electrical Engineering and Computer Science
May 22, 1998

Certified by .....
Clifton G. Fonstad
Professor of Electrical Engineering and Computer Science
Thesis Supervisor

Accepted by .....
Arthur C. Smith
Chairman, Department Committee on Graduate Theses

Characterization of Noise in Uncooled IR Bolometer Arrays

by

William Alexander Lentz

Submitted to the Department of Electrical Engineering and Computer Science
on May 22, 1998, in partial fulfillment of the
requirements for the degree of
Master of Engineering in Electrical Engineering and Computer Science

Abstract

An extensive noise analysis on an Uncooled IR camera was performed. Direct noise measurements on individual bolometers were verified, and several new experiments to reduce their noise were performed. The data shows that $1/f$ noise in bolometers can be substantially reduced by changing physical characteristics of the device. Noise tests on the overall system revealed the major sources of noise present in the system. A simple model was developed to provide a framework for discussing the system noise results. The major noise components were all identified and characterized.

Thesis Supervisor: Clifton G. Fonstad
Title: Professor of Electrical Engineering and Computer Science

Acknowledgments

I would like to deeply thank my company supervisor Neal Butler for his excellent guidance and support on my project. He was a mentor to me during my stay at the company, providing amazing help and quick insight into any problem I encountered. He always has a new and interesting problem or topic to discuss, and has a seemingly unlimited depth of knowledge.

I would also like to thank everyone who made my time at Lockheed Martin IR Imaging Systems a rewarding experience. Margie Weiler provided support and guidance during my first three summers. She gave me the technical background I needed to do my thesis. I am also grateful because she always had time to discuss things with me, and helped give me confidence by believing in me. I thank Margaret Kohin for her generous amounts of praise. She also often provided me with interesting projects to tackle during my time at the company. Nancy Hartle always greeted me in an enthusiastic and positive way. In addition, her practical help with reports and presentations are a valuable asset. Don Lee discussed numerous theories and ideas with me for long periods of time, even when swamped in other work. I appreciate his time and patience. Gary Tarnowski always provided help when I needed it and took time to learn about my projects. The people who helped me in lab are too numerous to list, but I want to thank the few who really spent a lot of time answering my questions: Bill and Pete in the Uncooled lab, and Bob and Karl in the HgCdTe detector test lab.

I thank Prof. Fonstad for keeping me on track with my thesis and his good nature about my delays.

Most of all, I would like to thank my parents. My mom got me to college and provided all the financial resources needed to keep me there. She sent plenty of cookies and gave me a lift whenever I was down. Best of all, she always has a ready ear when I need to talk. My dad supported me throughout college and gave lots of good practical advice about college and life. I also look forward to many more technical discussions with him.

Contents

List of Figures

List of Tables

Chapter 1

Introduction

Infrared (IR) imaging systems have found wide use in military applications, and are rapidly expanding in more commercial areas. Weapons sights and targeting systems equipped with IR sensors enjoy a significant advantage over non-IR systems. Reconnaissance and surveillance missions benefit from IR systems because they can operate in total darkness and through some obscurants such as smoke. Fire fighters want to use IR cameras to see through smoke, find fire burning behind walls, and determine if a floor is about to collapse because of fire damage. Non-contact radiometry could be used to monitor temperature-sensitive processes. Night-vision systems give drivers better vision on the road and help planes land at night.

For several decades IR imaging systems operating at cryogenic temperatures have been available. Recent advances in room-temperature microbolometer IR focal plane arrays promise performance similar to cooled systems at a lower cost and with smaller packaging. Bolometer arrays typically operate in the long-wave IR regime with wavelengths from 7-14 μm. Each bolometer is thermally isolated from its surroundings by a small bridge, supported by two thin legs. Each pixel is about 50 μm x 50 μm in area and 0.5 μm thick, yet microbolometers can typically withstand thousands of g's of shock.

Despite improvements in microbolometer technology, sensors have not reached theoretical performance levels. For a given set of optics, the ability to see an object clearly is limited by the sensitivity and noise of a device. Reducing system noise will

allow one to make out finer details and see smaller objects. The goal of this thesis was to measure the relative contribution of various noise sources and then determine what can be done to help reduce the noise. Both detector and read-out integrated circuit (ROIC) noise are important and were considered, but bolometer noise was a larger focus of the study.

Chapter 2 is concerned with testing individual bolometers without the complications of system noise. It begins with a brief review of bolometer terminology. Construction and verification of the test setup used in measuring bolometer noise is then discussed.

Chapter 3 presents the results obtained from testing a large number of bolometers. Various models are fitted to the data in order to determine the cause of the noise. Based on the results of testing, several new experiments were proposed to reduce noise. The results of one experiment are discussed.

Chapter 4 develops a basic framework for noise in the investigated Uncooled system. Two basic figures of merit for evaluating system performance are presented. The results of the system model are compared with data on numerous focal planes to ensure its validity.

Chapter 5 details how various components of the system noise were separated from one another. The major sources of system noise are identified and quantified. Suggestions on how to reduce the effect of most major noise components are presented.

Chapter 2

Single Element Testing

2.1 Overview

One main reason for testing individual bolometers is to obtain measurements free of the complications of system noise. If tests are only performed on a system level with all noise sources present, then it is often difficult to determine if the bolometer noise component has been correctly isolated. Constructing a test station capable of reporting the Johnson noise of resistors from 10 to 50 kΩ (roughly the range of resistance found in actual bolometers) requires a very low-noise amplifier, mainly because of the low frequencies involved. An ideal system would be able to measure Johnson noise to well below 0.1 Hz, but anything which performs well to about 1 Hz is adequate.

A general block diagram of the system used to achieve a low noise measurement is outlined in Figure 2-1. The test box is the most critical part of the testing. In an actual system, the parts are biased to about 1 μWatt, so the test box must be able to bias to this level. The test box also provides a gain of 1000 to bring the signal to a measurable level and create relative immunity against noise sources entering after its output. The two multimeters are used to record bias, measure bolometer resistance, and monitor output voltage for calibration of the test circuit. The Model 113 pre-amplifier serves mainly as a high-pass filter at the low end of the frequency measurement; the need for such a filter is discussed later. Since it has the capability,

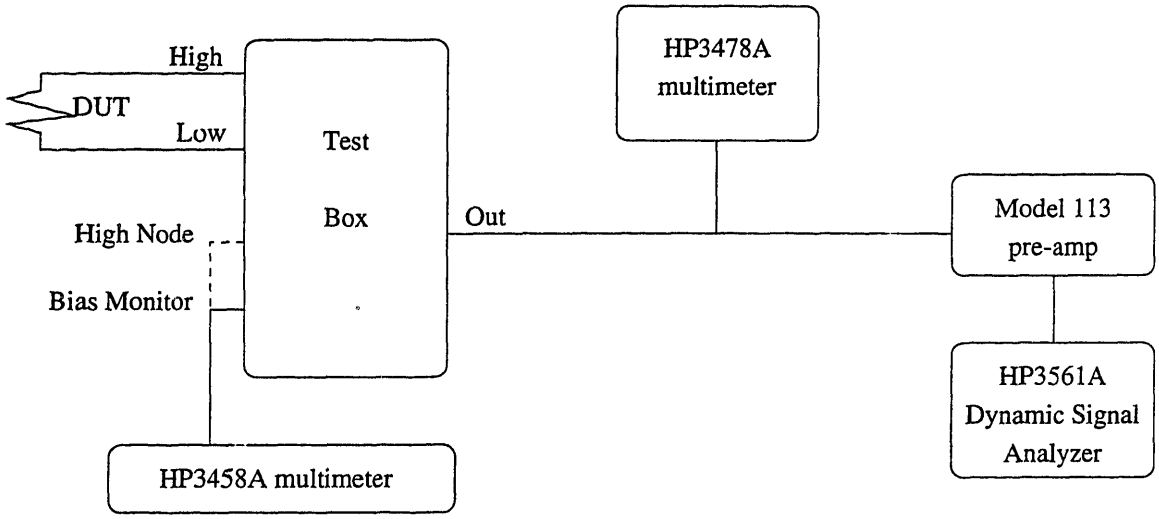

Figure 2-1: Test setup overview

the 113 amplifier can also be used for an additional gain of about 10 and low-pass filtering. The HP dynamic signal analyzer measures the noise power spectral density for bolometer noise.

There are several benefits to single element testing. As mentioned before, the interpretation of the results is relatively straightforward. In addition, single-element testing can be done at an early stage of device fabrication. If noisy parts are caught early, then costly processing steps can be eliminated for bad parts. The rapid feedback possible with this measurement enables a wide variety of testing to be performed in a short period without worrying about system noise fluctuations.

Testing individual bolometers cannot completely substitute for system-level testing. First, bolometers for testing are isolated so that metal contact probes can easily reach them. From photographs of parts, it is apparent that isolated bolometers often undergo a slightly different amount of etching than clustered pixel bolometers. Furthermore, test parts are located near the edge of an array, and only over a small region. If there is substantial variation across a wafer, then a few test parts may misrepresent the focal plane. System-level testing, backed solidly by testing of individual bolometers seems to be the best solution.

2.2 Bolometer Overview

A bolometer is a resistor whose resistance is a function of its temperature. Semiconductor bolometers usually drop in resistance as temperature rises, while metals exhibit the opposite behavior. By measuring the fractional change in resistance, one can measure a temperature change in the environment.

The bolometer technology investigated here was developed by Honeywell. A thin layer of vanadium oxide (VO_x) is sandwiched between two thin insulating layers. VO_x is a temperature-sensitive material, undergoing a larger fractional change in resistance for a given temperature change than many other semiconductors.

In order to achieve high thermal isolation, each bolometer is suspended above the substrate. Two small legs provide the only support for a bolometer (see Figure 2-2). Despite its precarious position, a bolometer is actually quite rugged because of the small scale.

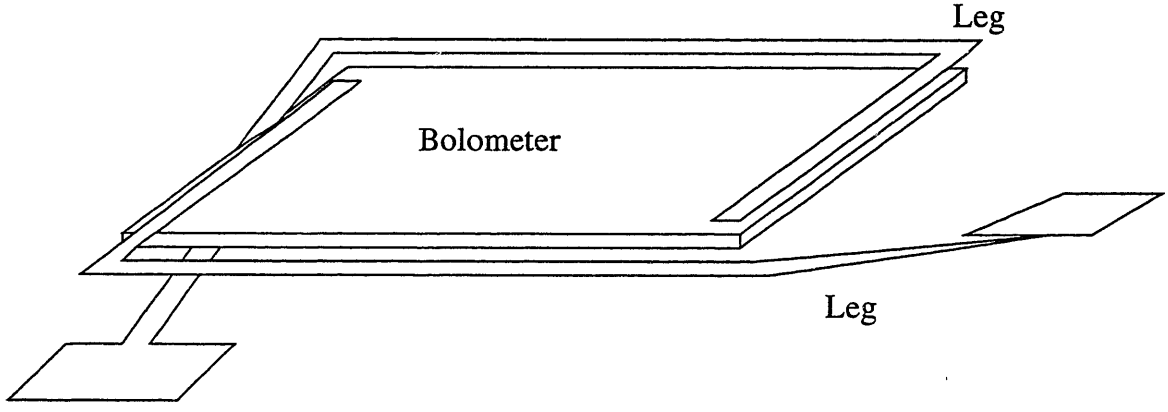

Figure 2-2: Single bolometer

Several terms need to be defined before going into any analysis on bolometers. The thermal coefficient of resistance (TCR) is a measure of the percentage drop in resistance per degree change in bolometer temperature. The equation for a semiconductor is given as [10]:

$$\text{TCR} = \frac{1}{R}\frac{\delta R}{\delta T} = -\frac{\beta}{T^2} \tag{2.1}$$

where β and R_o are constants dependent on a given semiconductor. Thermal capacity (C) is a measure of how much heat a pixel holds. It is similar to electrical capacitance, and is determined by device geometry and material. Thermal conductance (G) is a measure of how fast heat is transferred between a bolometer and its environment. For a given bolometer technology in a vacuum, G is mainly determined by heat transfer through the leg materials; radiative loss is negligible.

The response of a bolometer to a signal is given by [5]:

$$V_s = I\Delta R = IR(\text{TCR})\frac{P}{G} \tag{2.2}$$

where I is the current through the device, R is the bolometer resistance, and P is the power incident on the device.

Semiconductor bolometers with a negative TCR need to be tested with care; if one biases them too high, then an unstable condition causing burnout can be reached. As the resistance drops more current flows, leading to more Joule heating and a further drop in resistance. The cycle can continue until the device burns itself out.

Bolometer thermal characteristics determine the response time to a signal. τ, or the effective thermal time constant, is $\frac{G}{C}$. For the examined technology, τ is usually on the order of 10 ms, which substantially limits detector response time. For this reason, the examined bolometers can only be used in slow refresh rate systems (on the order of 60 Hz).

There are three main types of noise in semiconductor bolometers: white noise, flicker noise, and thermal noise. The white noise is Johnson noise, and appears in all resistors. Flicker noise has a $1/f$ noise spectrum and is usually linearly dependent on current. Thermal noise is caused by random heat exchange with the environment. The variance for each type of noise is given as [5]:

$$V_{white}^2 = 4kTRB_{white} \tag{2.3}$$

$$V_{1/f}^2 = \alpha V_{bias}^2 B_{1/f} \tag{2.4}$$

$$V_{thermal}^2 = \frac{4kT^2}{G} V_{bias}^2 (TCR)^2 B_{thermal} \tag{2.5}$$

where k is Boltzmann's constant, T is the bolometer temperature, B_{noise} are the noise effective bandwidths, α is an unknown proportionality constant, and V_{bias} is the bias on the bolometer. The thermal noise was never observed because of its low level (caused by a high G). Note that white noise can be easily separated from $1/f$ noise because of their different spectral characteristics.

When evaluating system performance, a better figure of merit to use is noise equivalent power (NEP). NEP derives directly from the voltage noise variance as follows [5]:

$$\text{NEP} = \frac{G}{\text{TCR}} \frac{V_n}{V_{bias}} \tag{2.6}$$

where V_n is the noise voltage. Assuming TCR and G stay relatively constant for a given process, a good noise figure of merit is V_n/V_{bias}.

2.3 Test Station Equipment

A test box was designed and built to measure Johnson noise on bolometers down to 1 Hz. The basic design consists of an N-stage parallel bridge circuit. By choosing an appropriate number of stages, one can optimize the noise characteristics of the overall amplifier for a given bolometer resistance. Using standard low-noise op-amps, an 8-stage design meets the required testing specification. One must be able to measure the Johnson noise on a 10-50 kΩ resistor to frequencies less than 1 Hz.

A diagram of 2 of N stages of the bridge circuit is shown below in Figure 2-3. Two inputs, "high" and "low," are connected to the bolometer, or device under test (DUT). Three outputs provide access to information which specify the operating parameters of the circuit. The "bias monitor" is the voltage across the top of the bridge, or approximately 11 times the voltage across the bolometer. The "hi monitor" is a direct measure of the bias across the bolometer. The "out" node is where the HP3561A makes its noise spectrum measurements. The DC level of the output gives feedback as to when the circuit is balanced. A low-noise voltage reference provides the bias voltage across the bridge. For the circuit to be balanced, the voltage across the DUT must equal the voltage across each 1 kΩ resistor. Adjusting the 500 kΩ

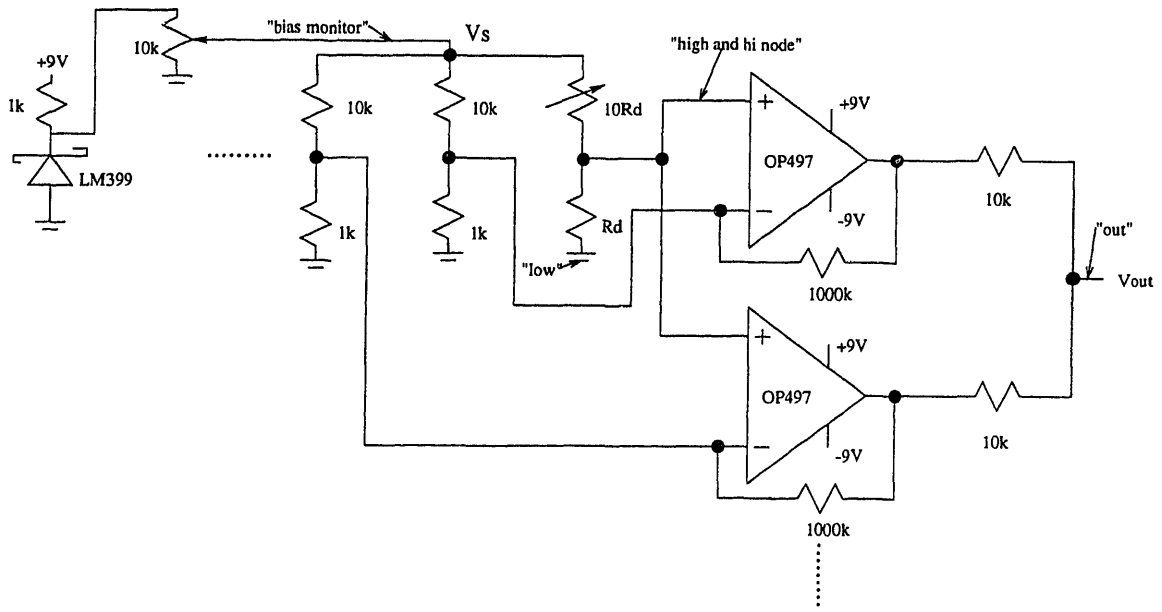

Figure 2-3: Bridge circuit : 2 of N stages

potentiometer until the DC output is 0 volts balances the circuit.

Motchenbacher and Connelly [8] provide a differential amplifier noise model, enabling one to estimate the performance of the noise circuit. The model for a single op-amp is shown below in Figure 2-4. Before drawing the equivalent noise model of

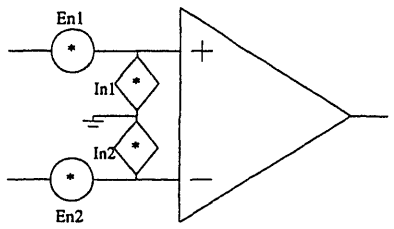

Figure 2-4: Differential noise model for an op-amp

the circuit, a small simplifying assumption will ease the analysis. The point labelled Vs in Figure 2-3 is approximately a voltage source with noise given by the voltage reference noise divided by the biasing potentiometer resistor ratio. For small changes in the DUT resistance the voltage at Vs will not change much, so the approximation holds.

Figure 2-5 below shows a noise equivalent model for one stage of the amplifier.

For simplicity, each noisy resistor has been replaced with a voltage noise generator and a noiseless resistor. For N-stages of Figure 2-5, and without connecting the

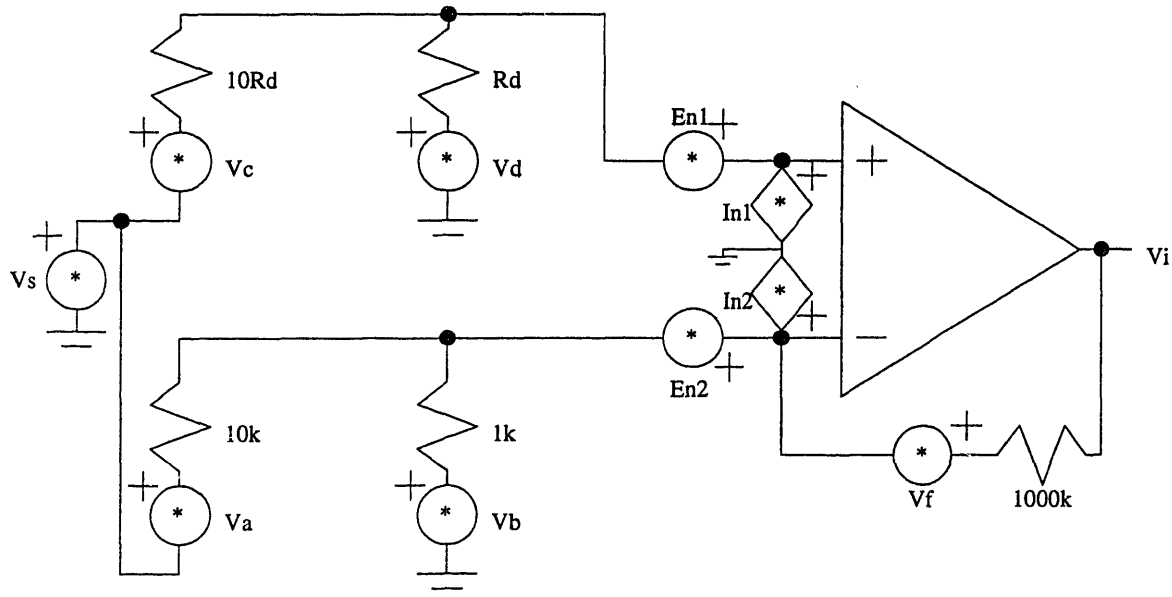

Figure 2-5: Noise model of 1 stage circuit

op-amp outputs together, the voltage at the output of each stage is given by (for $i = 1, 2, ..., N$):

$$\begin{aligned} V_i &= -100V_a - 1000V_b + \frac{1101}{11}V_c + \frac{11010}{11}V_d + \frac{1}{11}V_s + V_f + \\ &\quad 1101 \cdot (E_{n1} - E_{n2}) + N \cdot \frac{11010}{11}R_d I_{n1} - 10^6 I_{n2} \end{aligned} \tag{2.7}$$

Connecting all the op-amp outputs together through 10 kΩ resistors, and modeling each op-amp as a voltage source gives the following output voltage variance:

$$\frac{1}{N}\sum_{i=1}^{N} Var\,[V_i] \tag{2.8}$$

Finding the total variance requires one to determine which terms are correlated for the final sum. The correlated terms include V_c, V_d, and V_s since each op-amp sees the right half of the bridge in Figure 2-3 as the same. The current noise term involving I_{n1} is identical at each stage, so it does not average out. Uncorrelated terms include

V_a, V_b, V_f, E_n, and I_{n2}. The total variance at the output thus reduces to:

$$V_{total}^2 \approx \frac{10^4}{N}V_a^2 + \frac{10^6}{N}V_b^2 + 10^4 V_c^2 + 10^6 V_c^2 + 10^6 V_d^2 + 1/121 \cdot V_s^2 + \frac{1}{N}V_f^2 + \frac{1.12 \cdot 10^6}{N}E_n^2 + N \cdot 10^6 R_d^2 I_{n1}^2 + \frac{10^{12}}{N}I_{n2}^2 \quad (2.9)$$

The voltage noise terms are averaged out because they appear independently at the output of each op-amp. The current noise (I_{n1}) of each op-amp increases the total current noise of the circuit because all the terms are perfectly correlated (i.e., all the noise current flows through the DUT).

To achieve the necessary performance, parts were selected for their low-noise characteristics. Bypass capacitors installed on each voltage source reduced high-frequency noise. The OP497 op-amp was used in place of the AD745, even though the AD745 has better noise characteristics. Unfortunately, the AD745 had an unreasonably long delivery time, thus making the OP497 the only feasible choice. Chopper amplifiers also fell under consideration because of their low $1/f$ noise, but were rejected because of their high voltage noise. Too many stages would be required to reduce the voltage noise to an acceptable level.

Metal film resistors were used because they exhibit significantly less $1/f$ noise than carbon-based resistors. Three 9-volt batteries power the bridge circuit in order to avoid ground loops and 60 Hz power-line noise. One battery powers the LM399 voltage reference, and the two others provide the positive and negative polarity for each op-amp. The entire circuit is surrounded by a metal case which is tied to ground; thus some EMI is blocked by the case. The performance of the LM399 is adequate because its noise is not amplified at the output, as seen in Equation 2.9.

Carbon-based potentiometers, much like their resistor counterparts, are much too noisy for noise-sensitive applications. Two choices remain: cermet and wire-wound potentiometers. Wire-wound potentiometers tend to have the lowest noise, but are difficult to find in high-resistance values (i.e., 500 kΩ); therefore, Cermet potentiometers provide a good starting point. Selecting the potentiometer also required some thought into ease of testing considerations. To keep the DC output voltage from

changing less than 1 volt when $V_s \approx 4$ volts, the percentage change in the potentiometer resistance must be less than about 0.3%. In the worst case, the potentiometer resistance is as low as 100 kΩ, so adjusting to within 300 Ω may be necessary. Placing two 10-turn 10 kΩ potentiometers in series with the 500 kΩ potentiometer allows one to adjust within 500 Ω for half a turn, which is more than enough resolution.

2.4 Environmental Sources of Noise

Even if the electronic circuitry of a test station has negligible noise, one must be careful to reduce environmental sources of noise. Changes in the environment can generate false signals which show up as noise. For a test station, repeatability of measurements is a major concern.

One potential source of noise is microphonics. Microphonics are small vibrations in the environment which can produce noise in electronic circuitry. A common source of microphonics is motors. For example, a vacuum pump motor operated across the room from the test station generated a significant amount of noise.

Eliminating the microphonics noise allows one to get a better estimate of bolometer noise. Placing the entire test setup on a granite block reduced vibrations substantially. The granite block, with rubber padding beneath it, acts as a low-pass filter. A flexible padding beneath the test box itself further reduced vibrational noise.

Air currents flowing over a bolometer also posed a problem because they introduce a substantial amount of noise. Reduction of air currents was accomplished in a few ways. Enclosing the entire test setup in a box reduced air flow over the part; walking near the test station no longer generated spurious noise signals. More strict tests can be done to determine if environmental fluctuations are still a significant source of the measured noise. Placing the bolometers in a vacuum completely changes the amount of contact they have with the environment. If the measured noise is different on bolometers in vacuum and bolometers in air, then environmental fluctuations are a likely suspect. Another simple test involves measuring the noise on bolometers connected to the substrate and bolometers suspended over the substrate with

two thin legs (the standard configuration). If the noise changes dramatically, then environmental fluctuations are a potential cause.

Light also affects bolometer noise measurements. The measured resistance of an illuminated bolometer is different from the same bolometer in darkness. If a light source is not steady during measurement, then the resulting signal shows up as a substantial source of noise. For testing, the bolometers were kept in darkness.

Since a bolometer is thermally connected to its substrate, changes in substrate temperature may show up as noise. One solution is to place the substrate on a large block of metal; the large thermal constant of the metal prevents rapid temperature changes.

Electromagnetic interference (EMI) can also contribute to measured noise. Most commonly, radiated signals are picked up through loops of wire in the test setup. Ground loops were mostly eliminated by using a battery powered test box, thus reducing EMI. Placing the entire test setup in a metal box also reduced EMI since the box acts as a Faraday cage. Power line noise was not much of a problem, because the frequencies of interest were all below 40 Hz. The 60 Hz noise did not spill down into the 40 Hz range.

2.5 Filtering Out Unwanted Noise Sources

The spectrum analyzer computes an estimate of the power spectral density (PSD) over the frequency range of 0.1 to 40 Hz. A few artifacts may appear if care is not taken to appropriately filter the signal before processing. In particular, both high and low frequency content need to be considered to eliminate false results.

The signal from the test box must pass through a low-pass filter before it is sampled to avoid aliasing. Fortunately the HP3561A spectrum analyzer handles the anti-aliasing filter, so one does not need to worry about aliased noise.

Without a high-pass filter a low-frequency artifact shows up with a $1/f^2$ spectrum, thus covering the bolometer $1/f$ noise at low frequencies. The artifact arises because the temperature of a bolometer tends to drift slowly over time. For example, the

substrate may be changing temperature very slowly, or the bolometer may be heating its surrounding environment. The $1/f^2$ spectrum is greatly reduced by filtering out frequencies below 0.1 Hz.

Before sampling, filtering out frequencies below 0.1 Hz reduces PSD frequency components up to 10 or 20 Hz. This strange situation arises because two different time scales are involved in the measurement. In the continuous-time domain of the analog filter, the drift component of the signal is a ramp multiplied by a long "box." The Fourier transform of a long box (and its derivative) is concentrated very close to 0 frequency. Placing the drift through a high-pass filter with a cutoff of 0.03 Hz eliminates a significant part of the frequency components and thus most of the drift.

In the HP3561A, however, sampling only occurs for 10 s at a time when measuring frequencies down to 0.1 Hz. The slow ramp, if not filtered out in the continuous-time domain, appears as a ramp over a very short period of time. The discrete-time Fourier transform (DTFT) then becomes:

$$\frac{\sin\left(\omega\left(M+1\right)/2\right)}{sin(\omega/2)} \tag{2.10}$$

where $M = 400$ is the length of the sequence and k is the slope of the ramp. The DTFT has a much wider frequency content because of its short observation time. On a log-log plot of the PSD, the slope of the noise looks like $1/f^2$. The numerator of Equation 2.10 can be thought of as a modulation function, with the denominator acting as the envelope of the waveform. Ignoring the zero values caused by the numerator and remembering to square the function for the PSD, for ω much less than π the denominator has a slope approximately given by:

$$\frac{1}{(sin(w/2))^2} \approx \frac{4}{w^2} \tag{2.11}$$

Filtering out the slow ramp with an analog filter removes the unwanted $1/f^2$ behavior in the PSD. Care must be taken to prevent the $1/f^2$ artifact from overwhelming the real $1/f$ signal, so the signal was put through a high-pass with a cuton of 0.03 Hz (because it is the lowest cuton of the 113 pre-amp).

2.6 Data Fitting and Reduction

The data from the spectrum analyzer contains contributions from several unwanted noise sources, including test equipment noise. By fitting the data to a model and subtracting out the test equipment noise, one obtains a reasonably accurate measure of bolometer performance.

There are three main types of bolometer noise, all of which can be separately identified by their PSD characteristics: white Johnson noise, which has a flat PSD; flicker or $1/f$ noise, which has a $1/f$ spectrum; and thermal noise, which has a spectrum like bandlimited white noise. As noted before, the unique spectral shape of thermal noise was never observed, so it was not included in the model.

The test setup also contributes several types of noise to the measurement. Each op-amp has some white noise and some $1/f$ noise. Drift noise, as discussed before, may not be entirely filtered out by the analog high-pass filter, so it should be taken into account. Its PSD is approximately a $1/f^2$ spectrum (ignoring the zero points).

The types of noise mentioned above suggest a PSD model of the form:

$$S_{xx} = a^2 + b^2/f + c^2/f^2 \tag{2.12}$$

where a^2 is the white noise variance, b^2 corresponds to the $1/f$ noise variance, and c^2 belongs with the drift noise. For a positive bias on a bolometer, both a^2 and b^2 contain contributions from the bolometer and the test equipment. Separating the two components is discussed below.

The HP3561A spectrum analyzer provides a noisy estimate of the PSD. The data taken consisted of an averaged set of 16 periodograms, each with 400 frequency points, using a non-overlapping rectangular window. Some simplifying approximations help make the data fitting more tractable. First, each point of the data has an approximately Gaussian distribution. The actual distribution of each point is chi-squared, but it approaches the Gaussian distribution as more averages are performed. Also, the 400 points in each window of the periodogram are assumed to be relatively uncorrelated between windows so that each average is independent.

a^2, b^2, and c^2 can be found using a non-random parameter estimate method. Based on the model in Equation 2.12, the vector of data points may be thought of as:

$$\overline{y} = H\overline{x} + \overline{w} \tag{2.13}$$

$$H = \begin{bmatrix} 1 & 1/f_1 & 1/f_1^2 \\ & \vdots & \\ 1 & 1/f_N & 1/f_N^2 \end{bmatrix} \quad , \quad \overline{x} = \begin{bmatrix} a^2 \\ b^2 \\ c^2 \end{bmatrix} \tag{2.14}$$

where f_n is the n^{th} frequency point, $\overline{y}$ is a column vector of measured data points, and $\overline{w}$ is 0-mean Gaussian white noise with a covariance matrix Λ_w.

In order to solve the equation, Λ_w must be known. For Gaussian noise and large N, it can be shown that [7]:

$$var\left\{\frac{1}{K}\sum_{r=0}^{K-1} I_N^r\left(e^{j\omega}\right)\right\} = \begin{cases} \frac{2}{K}S_{xx}^2\left(e^{j\omega}\right) & \omega = 0, \pi \\ \frac{1}{K}S_{xx}^2\left(e^{j\omega}\right) & otherwise \end{cases} \tag{2.15}$$

where K is the number of averages and I_N^r is the r^{th} periodogram with N points. The variance of each periodogram point in Λ_w is approximately $\overline{y}$ divided by the number of averages performed (except at $\omega = 0, \pi$).

The probability density function (PDF) of $\overline{y}$ parameterized by $\overline{x}$ is given as:

$$p_{\overline{y}}\left(\overline{y};\overline{x}\right) \propto e^{-\frac{1}{2}(\overline{y}-H\overline{x})^T\Lambda_w^{-1}(\overline{y}-H\overline{x})} \tag{2.16}$$

To find the maximum-likihood (ML) estimate of $\overline{x}$, one must maximize $p_{\overline{y}}\left(\overline{y};\overline{x}\right)$. The resulting ML estimate is:

$$\hat{x}_{ML} = \left(H^T\Lambda_w^{-1}H\right)^{-1}H^T\Lambda_w^{-1}\overline{y} \tag{2.17}$$

The ML estimate is exactly the same as doing a weighted least-squares analysis of the data (using a statistical weighting). A standard least-squares fit would give undue attention to the lower frequency points because of their high noise levels. A weighted

least-squares fit gives equal attention to all noise levels.

Two important figures of merit for any estimator are bias and error covariance. The expected value of $\hat{x}_{ML}$ is $\overline{x}$, so it is an unbiased estimator. The covariance of $\hat{x}_{ML}$ is:

$$\Lambda_{\hat{x}} = \left(H^T \Lambda_w^{-1} H\right)^{-1} \tag{2.18}$$

The variance of a^2, b^2, and c^2 appear directly on the diagonal of the covariance matrix, so finding an error bound is relatively straightforward.

It is sometimes more convenient to express results in terms of standard deviations (a) instead of variances (a^2). To convert the error bound of $\hat{a}^2$ to an appropriate bound on $\hat{a}$, let $f = x^{1/2}$ and find how a small change in x affects f:

$$\frac{df}{dx} = \frac{1}{2\sqrt{x}} \quad \text{, thus} \quad Var\left[x^{\frac{1}{2}}\right] \approx \frac{1}{4\,\overline{x}}\, Var\left[x\right] \tag{2.19}$$

The above approximation only works if the variance of x is much smaller than its mean value. Since 16 periodogram averages were performed, the variance should be a factor of 16 below the mean, so the approximation is valid.

Some numerical simulation showed that the fit to data is somewhat lower than expected. The main reason for the error is because points with low values are given lower variance and thus a heavier weight. A spurious low point can drag down a measurement. By running the fitting algorithm more than once, one obtains a more accurate (i.e., less biased) fit to the data. The first iteration uses the data points over the number of averages as the variances. Each successive iteration uses the fitted curve of data points over the number of averages as the variances.

Once the noise data is fitted to $\hat{a}^2$ and $\hat{b}^2$, the test station noise should be separated from the bolometer noise. The bolometer $1/f$ noise separates easily from the test station $1/f$ noise when one considers data at 0-bias and a positive bias across the bolometer. There is no measured bolometer $1/f$ noise at 0-bias since no current is flowing through the part; therefore, subtracting the 0-bias value of $\hat{b}^2$ from the its corresponding positive-bias value yields the part of $\hat{b}^2$ from the bolometer alone.

Isolating the bolometer white noise is complicated because both the test station

and bolometer white noise are independent of bias. The measured white noise variance in a unit bandwidth is given by:

$$\sigma_w^2 \approx \frac{1.21}{16} V_n^2 + 16 i_n^2 R^2 + 4kTR \tag{2.20}$$

where V_n^2 is the op-amp voltage noise variance, and i_n^2 is its current noise variance. By observing the σ_w^2 for various values of R, one may approximately find V_n^2 and i_n^2. In addition, the OP491 data sheet provides a rough idea of what the two values should be.

2.7 Test Procedure

The test procedure followed is easy and yet provides all the essential quantities of interest. In addition, it gives a way to identify problem measurements during testing and allows verification of data during analysis.

The resistance of a test bolometer is measured for a given bias voltage. The bias voltage chosen is about 0.4 V (or about 0.04 V across the detector itself). The bias voltage is low enough so that heating of the bolometer is relatively negligible. After setting the bias, the bridge is balanced so the DC output level is 0 V. The top half of the bridge resistance (Rc) is now 10 times the bolometer resistance. Rc is measured by recording the voltage at the "bias monitor" node and then the current from the "hi node" when it is connected to an ampmeter. The DUT resistance (Rd) is obtained by taking the ratio of voltage to current.

Noise measurements occur at 3 bias points: 0, 1, and 1/4 μWatt. The 0 bias point gives the test box $1/f$ noise alone, along with a good measurement of the bolometer white noise. The 1 uWatt bias point is representative of the bias power used in actual operation of the device. The 1/4 μWatt bias point is useful because the applied voltage is half of its value at the 1 μWatt point. If the measured $1/f$ noise looks approximately 1/2 of its original value, then the measurement is probably valid.

2.8 Excess Noise

To verify the test station, noise on several metal-film resistors was measured. As bias increased on the resistor, $1/f$ noise increased as well. The measured $1/f$ noise should remain constant over all bias values unless the DUT has $1/f$ noise. Since metal-film resistors have low $1/f$ noise, the test station generated the extra noise. Replacing a part in the test box fixed the problem.

The source of the extra noise was the 500 kΩ Cermet potentiometer. Testing a 150 Ω resistor allowed the bridge to be balanced using one of the two smaller 10 kΩ potentiometers alone. No significant noise increase was observed from either small potentiometer. Testing a 21.5 kΩ resistor and using the large potentiometer resulted in a large increase in noise with increasing bias. Both burst noise and $1/f$ noise were present.

After a few other 500 kΩ potentiometers showed similar noise problems, a switched resistor network solved the problem. Six switches and resistors created a discrete potentiometer, with values between 0 and 480 kΩ at 20 kΩ intervals. The circuit is shown in Figure 2-6.

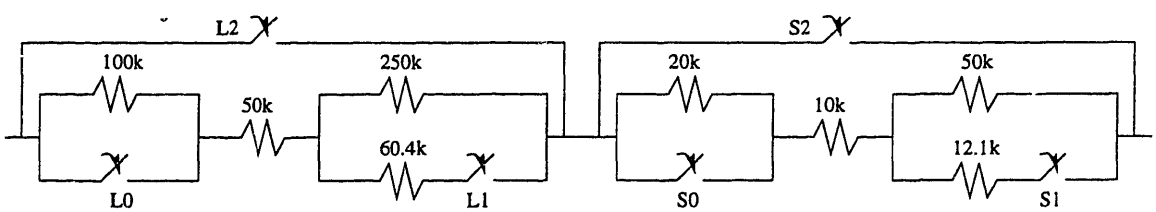

Figure 2-6: Switched resistor network

2.9 Test Pad Contact Noise

The test bolometers are not accessed in the same manner that bolometers in an array are. Test bolometers are wired directly to test pads on the side of a chip, while normal bolometers receive on-chip amplification before being measured. Test bolometers, because they receive no on-chip boost, are more sensitive to test pad

contact noise. Even if the test pad contacts are noisy, it is of no interest for the actual operation of the device.

A few different approaches were taken to verify that the measured $1/f$ noise was not due to contacts. First, data on normal metal-film resistors should show if there is a problem with the test station contacts themselves. Next, $1/f$ noise in the test pad contacts is a larger problem for low bolometer resistances. The noise figure of merit is V_n/V, which is proportional to R_n/R. An R_n term caused by the test pad contacts should be relatively independent of the bolometer resistance. For a given R_n, lower bolometer R increases the the noise figure of merit V_n/V if the problem is contact noise. A plot of the noise figure of merit vs. resistance is given in the following results section. In addition, the test pads were bonded with metal to another completely different kind of contact. The tests were then repeated under similar conditions for the same bolometers. If test pad contact noise were a problem, then some difference in the measured noise should be visible.

2.10 Results

2.10.1 Resistance Measurement

The resistance measured by the test box approximately corresponds with the resistance measured by an ohmmeter. Table 2.1 below gives a couple standard comparison measurements between an ohmmeter and the test station.

Ohmmeter R(kΩ)	Test Box R	Ratio
10.2	10.0	0.98
21.5	20.4	0.95

Table 2.1: Resistance verification

The accuracy of the test box has about a ±5% error. One reason for its inaccuracy is that voltage and current across the resistor are not measured simultaneously; loading of the test box by the current meter changes the operating point slightly.

2.10.2 Drift Reduction

Passing data through a high-pass filter reduces the drift component of noise substantially. Several parts have data both before and after the benefit of filtering. Table 2.2 below shows data for several representative parts, where "c" is the constant fitted to the $1/f^2$ noise component (see Equation 2.12).

Part ID	Type	"c"·10^7, no filter	"c"·10^7, with filter
20.08.04	F2	1.26	0.60
	F3	0.98	0.28
20.11.10	F2	1.23	0.28
	F3	1.07	0.23
20.11.05	F2	2.36	1.03
	F3	0.50	0.18

Table 2.2: Drift reduction

Drift noise initially is comparable with the $1/f$ noise at low frequencies, and thus it clouds a visual assessment of the noise. Reducing the drift noise component by a factor of 2-3 makes the noise look more $1/f$ and improves the $1/f$ fitting routine.

2.10.3 Validating the White Noise

Verifying that the white noise measured by the station is approximately correct helps validate the data collection process. Extracting the white noise of a bolometer requires a knowledge of the voltage noise of the op-amps. According to the OP491 specification sheet, current noise should only provide a $1/f$ component at low frequencies. Equation 2.20 shows the major components of white noise in the system.

Two methods were used to compute the white noise of the test box. First, measuring the noise on a known low-resistance metal-film resistor gives the voltage noise almost exactly. In this case, the measured white noise on a 150 Ω resistor was a total of 6.4 nV/$\sqrt{\text{Hz}}$. The actual white noise on the resistor is theoretically $\sqrt{4kTR} \approx 1.6$ nV$\sqrt{\text{Hz}}$, thus the total voltage noise is about 6.2 nV/$\sqrt{\text{Hz}}$. According to Equation 2.20, the variance on each op-amp is 16 times greater, so the noise per

root hertz is 4 times greater, or approximately 25 nV/$\sqrt{\text{Hz}}$.

To further verify the voltage noise measurement, white noise data on 100 parts was compared with the theoretical white noise value for each part. On average, the extra white noise was about 6.2 nV/$\sqrt{\text{Hz}}$; therefore, the two results agree very well. The OP491 data sheet confirms that the estimated voltage noise is reasonable. The data sheet specifies a typical voltage noise of 17 nV/$\sqrt{\text{Hz}}$ and a maximum of 30 nV/$\sqrt{\text{Hz}}$. The measured 25 nV/$\sqrt{\text{Hz}}$ lies comfortably in the data sheet range.

Figure 2-7 shows the distribution of ratios between the measured white noise (minus the test box voltage noise) and the theoretical white noise. The actual standard

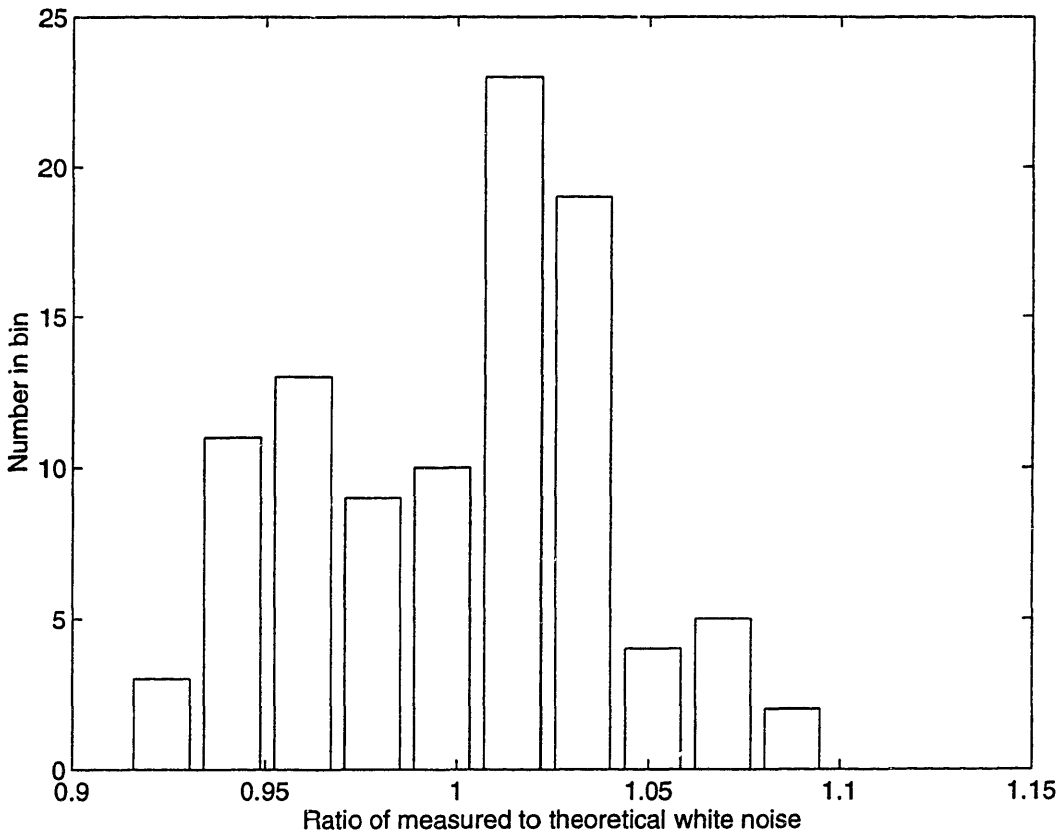

Figure 2-7: Histogram of measured / theoretical white noise

deviation on the measurements is about 4%, even though the predicted standard deviation is only about 1%. The measured resistance used for the theoretical white noise value is only good to within ±5%, and so it introduces more uncertainty.

2.10.4 Repeatability

One important aspect of any test is the ability to repeat results. The repeatability measurements done carry the idea even farther, as the parts were tested under two completely different environmental conditions. Bolometer response is very sensitive to the thermal conductance with its surroundings, thus testing the parts in air and in vacuum is a solid test to see if environmental fluctuations matter. In order to test parts under vacuum, the bolometer test pads had to be wire-bonded to a chip. As discussed before, if test pad contact noise were a problem then some difference should be observable in the measured noise.

The three conditions tested were: "Standard", "New Contacts", and "Vacuum." The "Standard" configuration means that the bolometers were tested in air with the normal test pad contacts. The "New Contacts" configuration was after the bolometer test pads had been wire-bonded to a chip, but the test was still performed in air. The "Vacuum" configuration occurred when the "New Contacts" parts were placed under a vacuum.

The graph in Figure 2-8 shows a normalized noise figure of merit (Vn/V) for each wafer tested. There are several parts on each wafer. For each part, the mean of Vn/V was taken across all measurements in different conditions. The Vn/V for each test was then divided by the mean. In an ideal case with perfect measurements, the resulting normalized noise figure of merit would be 1 for all the data points. With uncertain measurements, however, there will be some spread around 1. The vertical line in the graph is 3 standard deviations of the maximum predicted error (ignoring error in the calculated mean), so basically all of the data points should fall on the line. A small part of the data from the "Standard" configuration is more variable because it was not tested inside a box. When people walked by, the noise would increase a little bit, thus giving a few scattered high points on the graph which do not lie within the predicted error. A single high point is enough to disturb the calculated mean and cause a few points to fall below the error bound as well.

As shown in Figure 2-8, the results from the two thermal environments are ba-

sically the same. The unchanged results given a large change in the environment strongly suggest that environmental fluctuations do not contribute significantly to the measured $1/f$ noise.

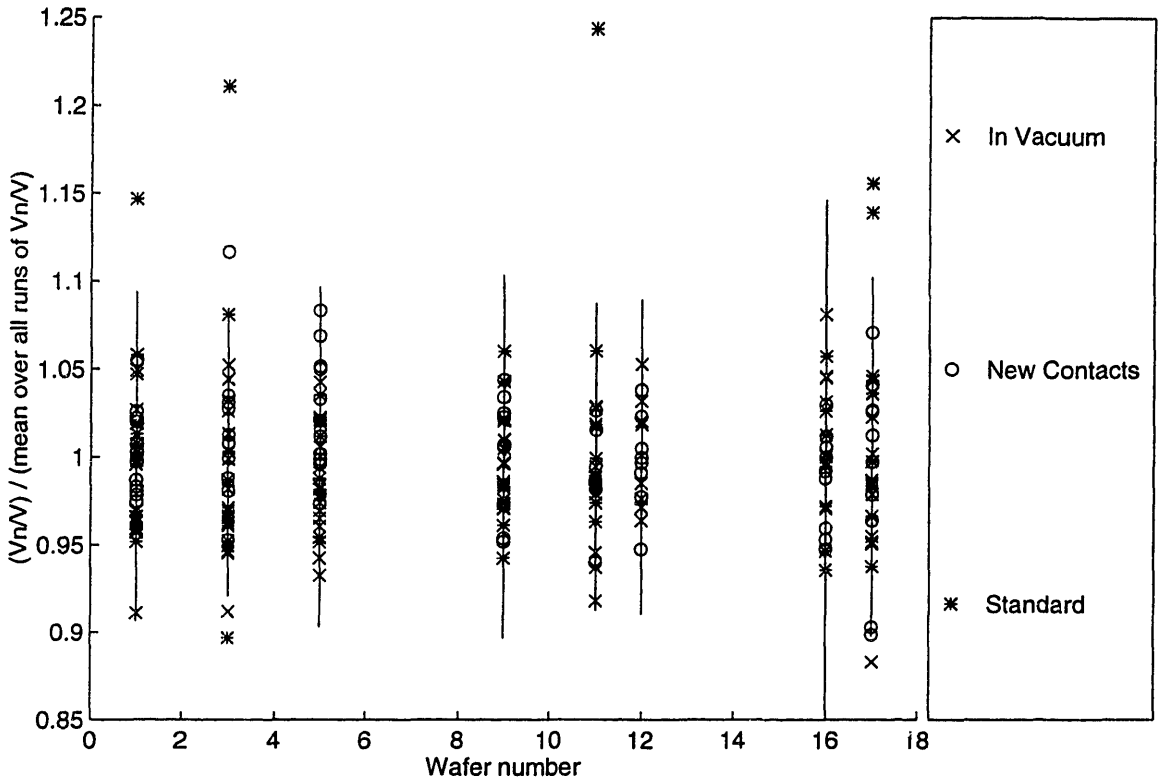

Figure 2-8: Repeatability test

2.10.5 Excess Test Box $1/f$ Noise

The $1/f$ noise of the test box alone should not change with bias. By testing a metal film resistor with low $1/f$ noise, one can see if any resistors in the test box exhibit $1/f$ noise. The first round of tests showed that $1/f$ noise increased strongly with bias (see Figure 2-9). Replacing the 500 kΩ potentiometer with the resistor network described in Section 2.8 virtually eliminated the problem; $1/f$ noise becomes independent of bias (see Figure 2-9).

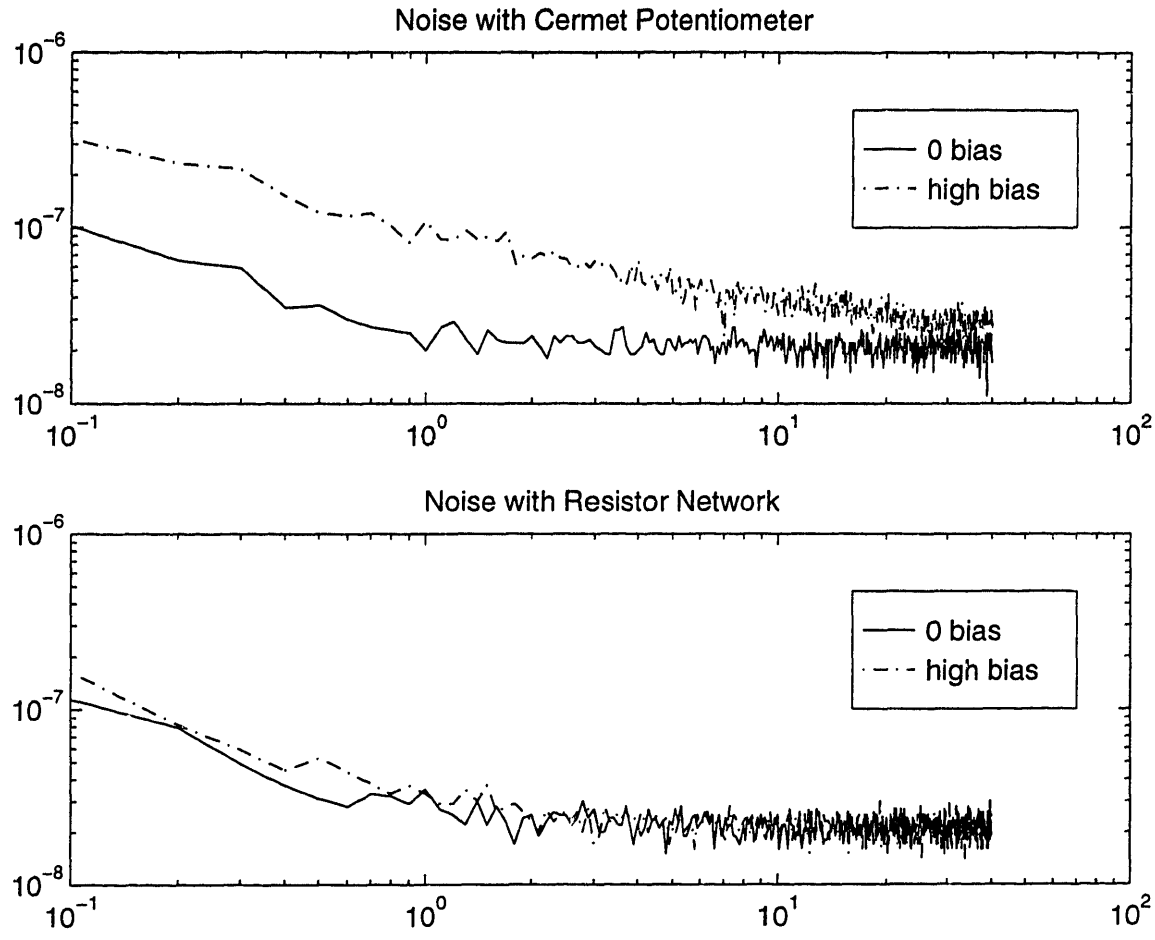

Figure 2-9: Test box $1/f$ noise and bias

2.10.6 $1/f$ Dependence on Current

$1/f$ noise typically scales linearly with current. Since all parts were tested at two biases (plus a 0-bias), it was easy to verify that the measured $1/f$ noise did in fact scale linearly with applied voltage (and thus current). Figure 2-10 shows a normalized noise plotted versus a normalized bias voltage. For each part, the two measurements were normalized to the noise and bias level of the lowest measurement.

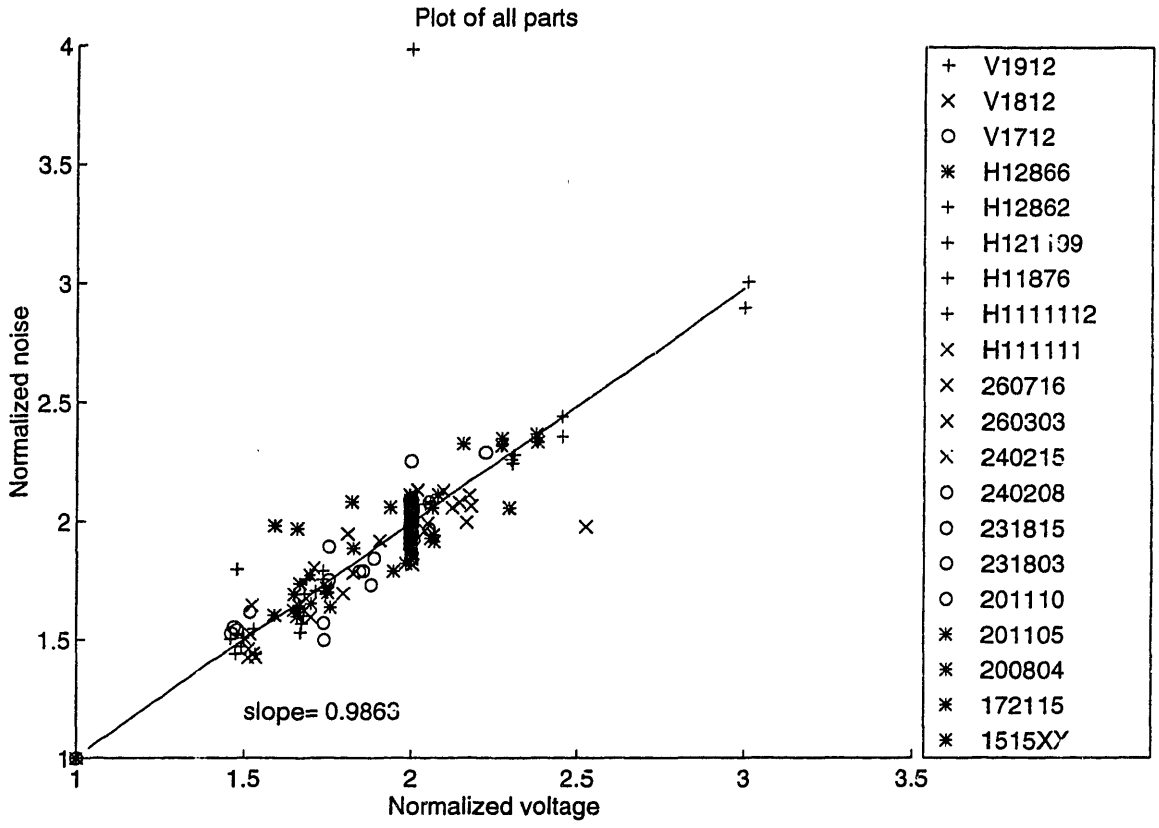

Figure 2-10: Linear dependence of $1/f$ noise on current

2.10.7 Contact Noise

Test pad/test probe contact noise does not affect the measurements taken. As seen in Figure 2-9, normal resistors showed no excess $1/f$ noise; therefore, they had no test probe contact noise. In addition, lower resistance parts should be more affected by contact noise. Figure 2-11 shows that $\Delta R/R$ actually decreases as R decreases, thus test pad contact noise is not present. Further evidence that contact noise is not a measurable source of noise is presented later.

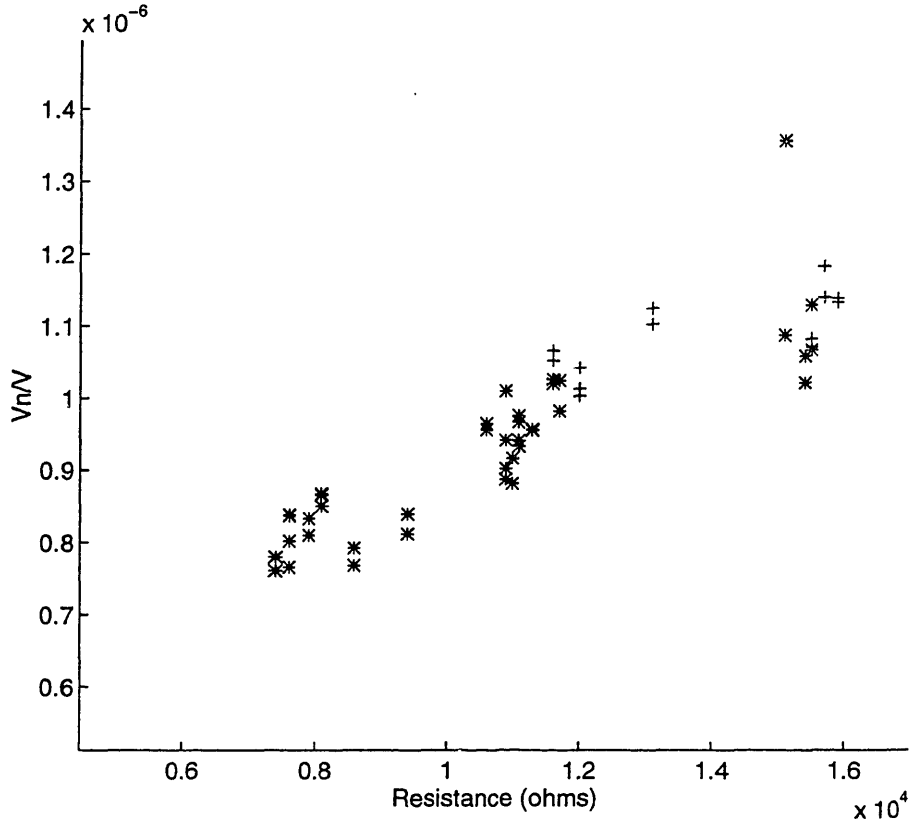

Figure 2-11: Contact noise test

Chapter 3

Bolometer Tests

3.1 Overview

Verification of the test procedure paves the way for extensive testing on parts in hopes of finding the cause of $1/f$ noise. The magnitude of the $1/f$ noise can be put into system models where its relative importance can be determined. The main goal of testing is to find how much $1/f$ noise affects system performance, and how to reduce its impact.

There are several advantages to single element testing over system testing. Parts that do not work in an actual system can still be characterized by a robust test station. The wider range of experiments possible gives more information on determining how to reduce $1/f$ noise. Also, the rapid feedback possible allows more data to be collected without spending time and money on building entire systems. Analysis of single element testing is much simpler than analyzing an entire system.

The main strategy consisted of testing a large number of parts fabricated over an extended period of time. If any change is visible, then it may be correlated back to a change in a processing parameter. The main process changes observed include variations in pixel geometry, resistance, thickness, and stress. Except for thickness, most process variations are present on every wafer manufactured.

3.2 Background on $1/f$ Noise

Flicker noise, or $1/f$ noise, has been observed in a wide range of systems, from the height of the Nile river over the last century to semiconductors. Despite its ubiquitous presence, there is no unified theory for its source in semiconductors. Its main characteristic is a $1/f$ power density spectrum (PSD) down to any measurable frequency. $1/f$ noise is usually observed as a voltage or current fluctuation. Clarke and Voss [9], however, showed that it is really a resistance fluctuation that causes $1/f$ noise.

Hooge's empirical model characterizes a wide range of noise in metal films with only a single fitting constant. The formula for the normalized resistance PSD is given by [11]:

$$\frac{S_R(f)}{R^2} = \frac{\alpha}{Nf} \tag{3.1}$$

where $S_R(f)$ is the resistance PSD, R is the resistance, $\alpha \approx 2 \cdot 10^{-3}$ is a fitting parameter, and N is the number of carriers in the sample. Although Hooge's model works well for metal films, it doesn't always work for other materials. Hooge's formula is commonly thought of as a volume effect, since N is proportional to the volume of the resistor.

Another important set of experiments on $1/f$ noise came from Clarke and Voss. They hypothesized that $1/f$ noise may arise from spontaneous temperature fluctuations in a material. The temperature fluctuation model has an interesting consequence for bolometers, since a higher TCR (temperature coefficient of resistance) will lead to more noise as shown below:

$$\frac{\Delta R}{R} = (\text{TCR})\Delta T \tag{3.2}$$

where $\frac{\Delta R}{R}$ at 1 Hz is equivalent to the noise figure of merit. The above equation is a direct result from the definition of TCR (see Equation 2.1). As evidence for their model, Clarke and Voss observed that manganin, which has a TCR of virtually 0, has no measurable $1/f$ noise. The temperature fluctuation model is also a bulk effect; it

goes down as volume increases.

3.3 Tested Parts

Standard test bolometers are fabricated on the side of every wafer to allow resistance, TCR, and other basic parameter measurements. Testing standard parts has the advantage of being able to examine parts ranging over a wide period of time. With a large amount of data, correlations between processing parameters and noise are more likely to show up. Unfortunately, the test bolometers were not designed with noise measurements in mind; therefore, sometimes different test pixels do not give significantly different information.

For the test pixels, a few basic parameters were varied. The parameters include geometry, contact area, and isolation/stress. None of the pixels are rectangular, but for simplicity their shape can be approximated with a rectangle having some effective width and length. Before etching, pixels are connected directly to the substrate. After etching, pixels are suspended above the substrate by two thin legs. On each wafer, pixels connected to the substrate and suspended pixels are present. For standard testing, the 6 types of pixels are: F2, F3, F2L, F3L, F5, and F6. The differences in important parameters for each pixel type are given in Table 3.1.

Pixel	l (shortest)	$w_{contact}$	Suspended?	R
F2	15	38	yes	1.4
F3	15	38	no	1
F2L	27	19	yes	4
F3L	27	19	no	2.7
F5	14	22	yes	1.5
F6	14	22	no	1.1

Table 3.1: List of part types

A "yes" to "suspended?" means the pixels have been etched away from the substrate, R is the approximate resistance, l is shortest distance between the two contacts, and $w_{contact}$ is the width of the contacts (or size along the bolometer width). The

resistances given are relative to the smallest value.

One important feature of Table 3.1 is that the resistance for parts with the same geometry (e.g., F2 and F3) is not constant. To suspend parts above the substrate, a layer of material is etched out. After etching, the resistivity of a part changes.

There are a number of difficulties with Table 3.1. First, the effective width and length of any pixel is not known. The values in the table give a length and width which should be roughly proportional to the actual size of the device. Also, pixels have corners, meaning that the current flow through them is not uniform. For simplicity, all models assume that the current flowing through a device is uniform. Next, the two contacts do not have a constant distance between them. It is often difficult to find the exact fraction of the contact area that has a significant amount of current flowing through it relative to the rest of the contact. From pixel design to pixel design multiple things change at the same time, thus clouding analysis. In future tests, only one variable should be changed between pixels. Designing a simple geometry (i.e., rectangular) would further clarify test results.

Two new pixel types were also tested. Fortunately the new pixels have varying thicknesses, an ideal test for differentiating between noise models. The two new pixels are L1 and L2. The L1 pixel is the same as the F2L pixel and serves as a control in the experiment. The L2 pixel is somewhat smaller than the L1 pixel. The approximate properties of each pixel are summarized in Table 3.2 below. The three wafers, V1712, V1812, and V1912, have VOx thicknesses of about 1000, 500, and 250 Angstroms, respectively.

Pixel Name	l (shortest)	$w_{contact}$	Suspended?	R
F1	27	19	yes	4
F2	13	12	yes	2.8

Table 3.2: List of new part types

3.4 Simple Noise Models

A few models of $1/f$ noise are needed to gain a straightforward understanding of the behavior of $1/f$ noise under different assumptions. The goal of such models is to help analyze data and find out where the noise is coming from. In addition, having a simple model allows one to envision many different process variations which will distinguish between different types of noise.

One likely model for $1/f$ noise is a bulk effect, where the noise is generated uniformly throughout the resistor. For a bulk effect, the noise can vary as:

$$\mathrm{NF} = \frac{V_n}{V_{bias}} \propto \frac{1}{\sqrt{V}} \tag{3.3}$$

where $V_n = \sqrt{S_V(f=1)}$, V_{bias} is the voltage across the resistor, and V is the volume of the sample.

The two basic quantities returned from each measurement are the noise figure of merit (NF) and resistance (R). The NF is related to the resistance through two equations. The resistance of a bolometer is:

$$R = \rho \frac{l}{wt} \tag{3.4}$$

where ρ is the resistivity, and l, w, t are the length, width, and thickness of the device, respectively. Combining Equation 3.3 with Equation 3.4 results in the following relation:

$$\mathrm{NF} \propto \frac{1}{\sqrt{wlt}} = \frac{\sqrt{R}}{l\sqrt{\rho}} \tag{3.5}$$

Unfortunately, Equation 3.5 depends on the length of the bolometer l. When testing various geometries, it is nice to normalize out the effect of having different lengths so that intrinsic material quality can be compared. Using Table 3.1, one can multiply $\mathrm{NF}/\sqrt{R}$ by its approximate length to get rid of the dependence on l.

Another way to view noise is with a simple circuit model. Often, a simple resistor-based model is much clearer than a formula. For example, one can find the effect of

doubling the thickness of a resistor. Let the initial noise figure of merit be $\frac{V_n}{V} = \frac{I_n}{I} = \alpha$. Doubling the thickness of a sample is equivalent to having two resistors connected in parallel, each with the same noise and resistance. The variance of the noise current through each resistor adds, so the new noise figure of merit is $\frac{I_n}{I} = \frac{\alpha}{\sqrt{2}}$. As before, the noise goes down as the square-root of the thickness.

Another model for noise is a surface layer picture. The material near the surface of a bolometer undergoes a more rigorous treatment than the bulk, so it may be more noisy because of damage. Bolometers are especially sensitive to surface effects because they are typically extremely thin (on the order of a few hundred Angstroms thick). The circuit model for a surface layer effect is two resistors in parallel. One resistance is due to the surface layer and generates noise, while the other resistance is the bulk resistance with no noise.

Assuming the bulk and surface resistivity are the same, the noise figure of merit works out to be:

$$\mathrm{NF} \propto \frac{1}{\sqrt{wlt_s}} \cdot \frac{1}{1 + t_b/t_s} \tag{3.6}$$

where w is the width of the bulk and surface, l is the length of both sections, t_b is the bulk layer thickness, and t_s is the surface layer thickness. Using the above equation, the following relation between the noise figure of merit and R arises:

$$NF \propto \frac{1}{l\sqrt{\rho}} \sqrt{\frac{t_s + t_b}{t_s}} \cdot \sqrt{R} \tag{3.7}$$

Again, thickness is fixed, so the length can be normalized out in the same fashion using Table 3.1.

Several observations need to be made about the above equations. First, for a fixed thickness, there is no way to distinguish between a surface layer and a bulk effect by varying width and length alone (and given only NF and R). Next, the surface layer model (Equation 3.6) predicts that noise will go down as $\sqrt{t_s}$ when $t_s \gg t_b$, and noise will go down as t_b if $t_b \gg t_s$. The ratio of the bulk thickness to the surface thickness determines how fast the noise drops as the thickness of a sample increases. Again, for simplicity the model assumes that the resistivity of the surface and bulk are the

same, even though it may not be true in an actual bolometer.

Contacts are an observable source of noise in many devices, so another potential model involves contacts. As previously described, the test pad contacts were ruled out, but the contacts on the actual bolometer were not discussed. The circuit model based on contacts is two resistors in series, with the contact resistance given by R_c and the bulk resistance given by R_b. For simplicity, the two contact resistances are lumped together into one resistor. The bulk of the bolometer is assumed to contribute a negligible source of noise.

The approximate NF, given that the measured contact resistance is much lower than any bolometer resistance, is given by:

$$\mathrm{NF} \propto \frac{1}{\sqrt{Area_{contact}}} \frac{R_c}{R_b} \tag{3.8}$$

Note that as the bolometer resistance drops, contact noise becomes a larger problem. It is approximately true for all the measured devices that the contact width is the same as the bolometer width. With this assumption, the following relation arises:

$$\mathrm{NF} \propto \left(\frac{1}{wl_c}\right)^{(3/2)} \cdot R \tag{3.9}$$

For the contact model, a plot of NF normalized by R is more appropriate than a plot normalized by $\sqrt{R}$. As the width of the device goes up, NF/R should drop. Since all the contact lengths are the same, one can use Table 3.1 to normalize out the width of the device (by multiplying by $w^{3/2}$).

For all the above models, resistivity does not affect the noise figure of merit. If one assumes that the noise varies with the carrier concentration (N) as $1/\sqrt{N}$ instead of with the volume as $1/\sqrt{V}$, however, resistivity plays an important role in noise measurements. The noise figure of merit is now given as $\mathrm{NF} \propto \sqrt{\rho/(wlt)}$. Solving for the new dependence of NF on R and assuming a bulk effect model gives:

$$\mathrm{NF} \propto \sqrt{\frac{R}{l}} \tag{3.10}$$

If the noise figure of merit is a function of resistivity, then all the ρ terms disappear when NF is divided by $\sqrt{R}$. Since resistivity changes when parts are etched, it is possible to distinguish between the volume and carrier concentration models.

3.5 Estimating Geometry with Noise

One extra application of noise measurements is that they allow one to estimate the length and width of a bolometer's electrically active area. If the model for noise is known, then the results are relatively straightforward to interpret. If the approximate length and width of a pixel are known, then the estimation based on different models serves as a validation check for each model. If one has a simple pixel, then its length and width are easily compared to more complicated geometries; thus, one can get a better estimate of the properties of complicated geometries.

The three basic models for noise are developed in Section 3.4. For a bulk noise effect, Equations 3.3 and 3.4 lead to a set of equations for length and width as given below:

$$l \propto \frac{\sqrt{R}}{\mathrm{NF}} \quad \text{and} \quad w \propto \frac{1}{\mathrm{NF}\sqrt{R}} \cdot \frac{\rho}{t} \tag{3.11}$$

The exact relation between l and the two measured quantities R and NF may be found, but it is often more useful just to compare how the length and width change from a standard simple geometry. If one pixel is rectangular and another has a complicated shape, then taking the ratio between the lengths of the two pixels gives an effective length for the complicated geometry. Note that the width equation depends on ρ and t while the length equation does not; therefore, the width should only be compared between pixels having the same resistivity and thickness.

Similar equations may be found from the various other noise models. For completeness, the length and width equations are given below in Table 3.3.

Several features of the above models are worth noting. First, it is not possible to distinguish between the bulk and surface layer model from length and width estimates alone. By varying thickness, however, the difference becomes apparent. The contact model, as before, has a very different behavior than the other two models. Its

Model	w	l
Surface layer	$\propto \frac{\sqrt{R}}{NF}$	$\propto \frac{1}{NF\sqrt{R}}$
Contact	$\propto \left(\frac{1}{NF \cdot R}\right)^{2/3}$	$\propto \left(\frac{\sqrt{R}}{NF}\right)^{2/3}$

Table 3.3: Length and width estimates

properties easily distinguish it from the bulk and surface models, even if only width and length variations are present.

3.6 Results

The results come in two main segments. The first part is a large amount of data from standard parts, which can only distinguish between bulk/surface layer and contact effects. The second part is a small amount of data on non-standard parts with varying thickness, thus enabling one to distinguish between surface layer and bulk effects. The surface layer model fits all the available data most closely. Unfortunately, the small data set coupled with the relatively large number of unknown parameters means that no model is certain. More tests need to be performed. The tests do, however, show that noise can be substantially reduced by changing certain pixel parameters.

Over 100 parts were tested at 3 bias voltages for the standard geometries, namely F2, F2L, F3, F3L, F5, and F6. The two basic parameters extracted from each set of 3 measurements are a noise figure of merit (NF) and resistance (R). Figure 3-1 shows the two parameters plotted against one another. For the standard parts, the results fall into two groups. Each group's noise varies with resistance, but not with resistance between groups.

The plot of the noise figure of merit normalized to pixel length and resistance is shown in Figure 3-2. The relative pixel lengths were taken from Table 3.1. The relatively flat result is in agreement with Equations 3.5 and 3.7, thus indicating that a bulk or surface layer model is appropriate. Furthermore, because the F2/F3 and F2L/F3L groups have the same normalized noise in the plot despite their completely

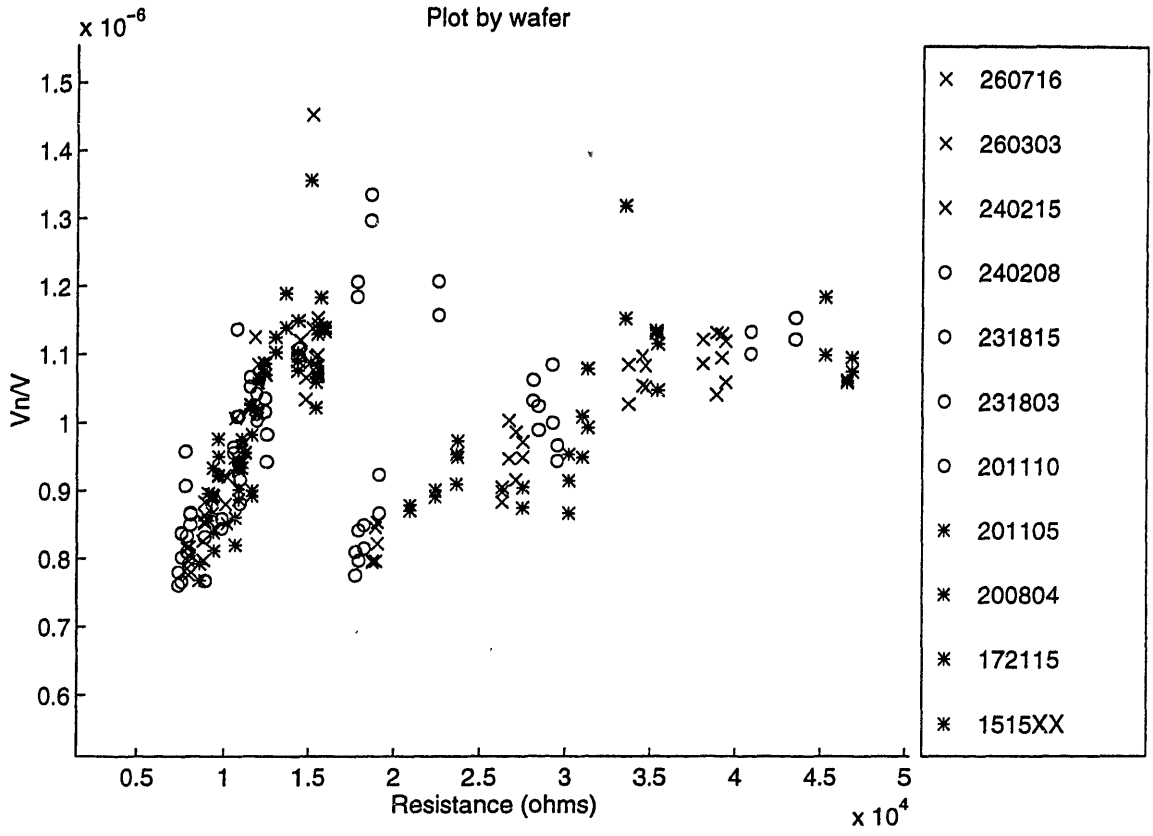

Figure 3-1: Experimental results on standard parts

different resistivity, a model in which noise varies with resistivity (see Equation 3.10) seems appropriate. If all the resistance variation is due to carrier concentration and not thickness or mobility variations, then the Hooge model fits well. Note that the relative height of the groups may be slightly off because the part width and lengths are only known approximately.

The contact model is ruled out by Figure 3-3's disagreement with Equation 3.9. If a contact model were valid, then the resulting plot would be flat within a given type of pixel, even if the widths were totally unknown.

Given the validity of the bulk or surface layer noise model, it is possible to estimate the ratio between the width and length of each part using Equation 3.11. Since the width equation is not independent of ρ, only pixels that are both etched or both not etched are compared. Table 3.4 gives a summary of the relative lengths, and Table

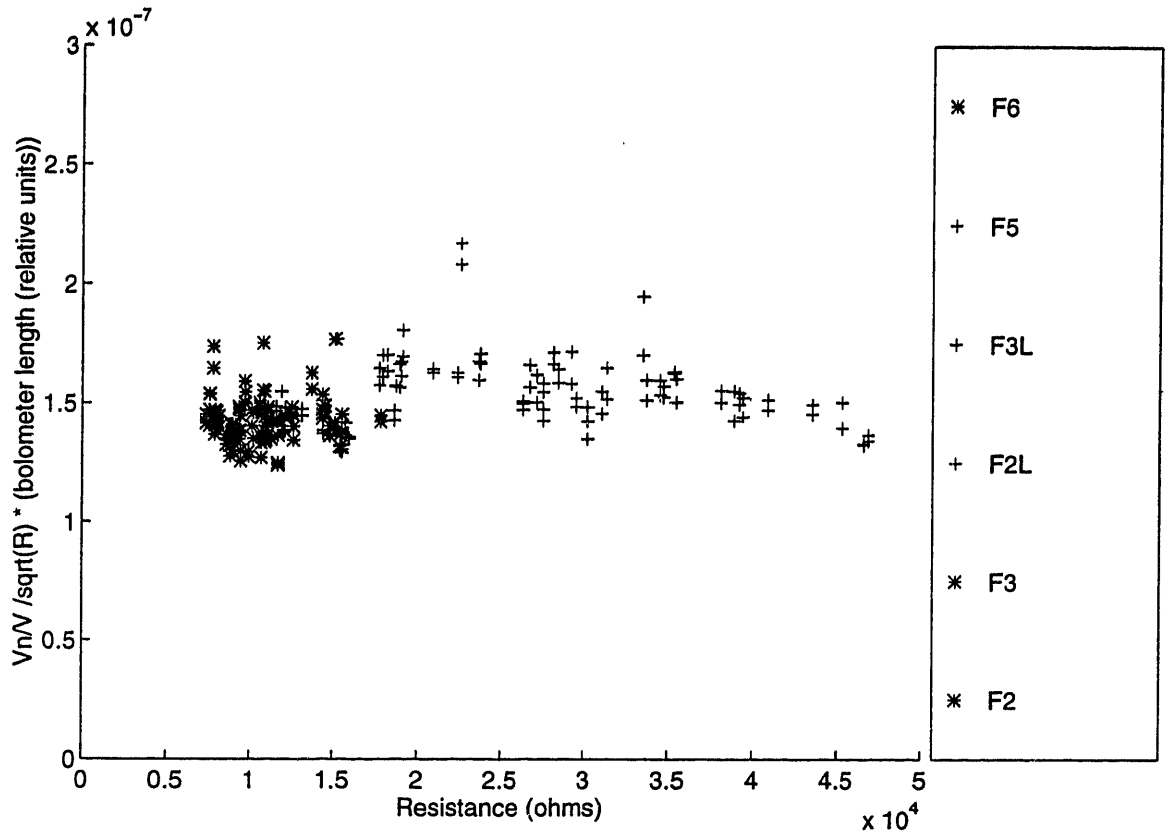

Figure 3-2: Bulk model scaling on standard parts

3.5 gives the relative widths. The information agrees fairly well with the shortest lengths and contact widths given in Table 3.1. The length ratio between F3L and F3 should be around 1.8, and should be the same for the ratio between F2L and F2. The length ratio between F6 and F3 (or F5 and F2) should be about 0.9. The width ratio between F3L and F3 (or F2L and F2) is about 0.5, and the ratio between F6 and F3 (or F5 and F2) is around 1.2. The approximate agreement between pixel sizes and predicted pixel sizes gives more weight to the bulk/surface layer model for noise.

Based on the above results, several new experiments were proposed. Time only allowed for a small subset of the proposed experiments, which involved testing parts with different thicknesses. The thickness experiment consists of a small set of data taken from 3 wafers. The overall plot of the noise figure of merit versus resistance is shown in Figure 3-4. The most striking feature of the plot is the much wider range

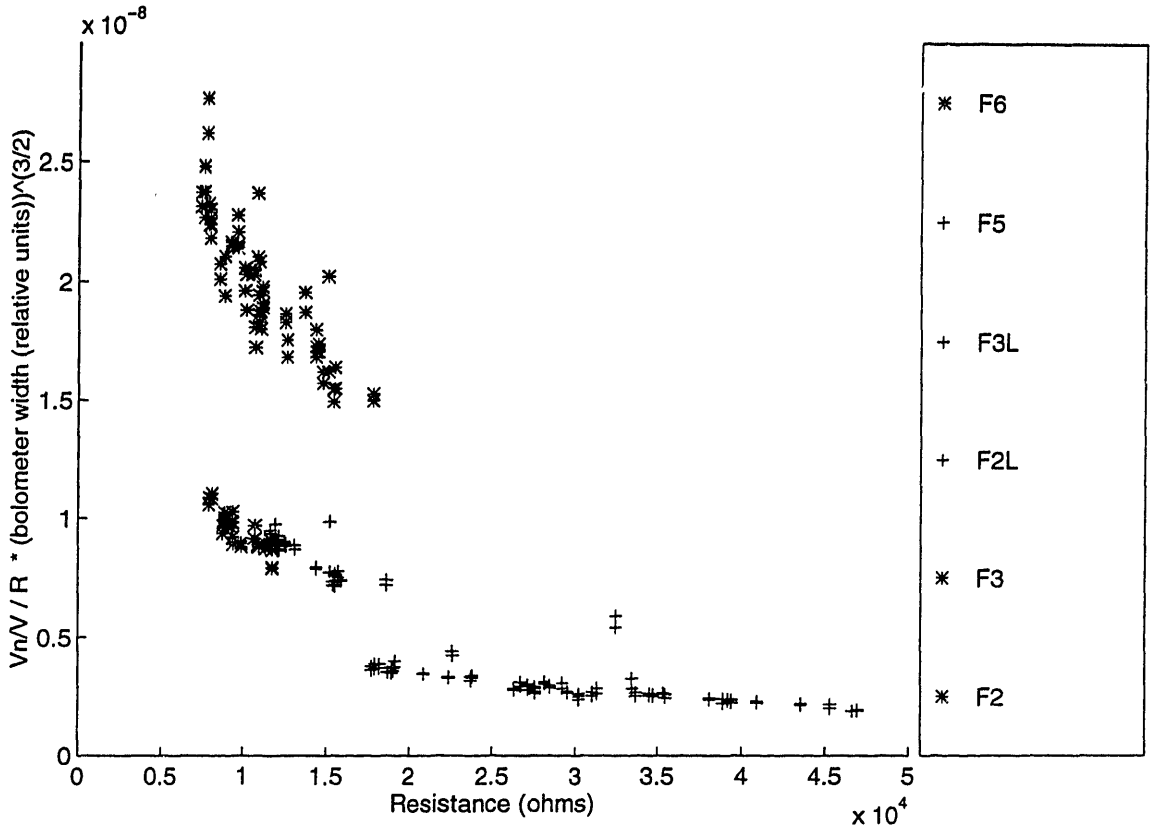

Figure 3-3: Contact model scaling on standard parts

of variation in NF. NF goes down as the thickness increases.

Since the contact model has been ruled out based on previous experiments, the plot proving its failure for the experimental parts is not shown. Different thicknesses should allow one to distinguish between the surface layer and bulk models of noise, however. A plot of NF/$\sqrt{R}$ normalized by length is given in Figure 3-5. For thin parts, the noise follows the bulk model and is constant. For very thick parts, however, the noise goes down faster than the bulk model predicts. The surface layer model explains the data in this case. For thin parts (V1812 and V1912), the surface layer thickness extends throughout the entire sample; therefore, the phenomenon is essentially bulk. For thick parts (V1712), the surface layer is more comparable to the bulk thickness, so noise goes down slightly faster than the bulk model predicts, as shown in Equation 3.7. If the thickness is increased enough, then the noise figure of merit will be inversely

Part 1 Relative to Part 2	Relative Length
F3L / F3	1.5
F6 / F3	1.0
F2L / F2	1.7
F5 / F2	1.1

Table 3.4: Relative lengths

Part 1 Relative to Part 2	Relative Width
F3L / F3	0.6
F6 / F3	0.9
F2L / F2	0.6
F5 / F2	1.0

Table 3.5: Relative widths

proportional to the thickness of the sample; otherwise for small thicknesses, NF goes down as the square root of thickness.

Despite the apparent success of the surface layer model, one must observe that only 3 real data points with thickness are available. Further testing needs to be done before any final conclusions are reached. There are many experiments under consideration. Further thicknesses need to be measured, along with different surface preparation techniques.

In conclusion, the measurements on a large number of test pixels ruled out contacts as a source of noise completely. The preliminary experiments begun with thickness variations suggest that noise is confined to some region near the surface of a bolometer. Noise does appear to be a function of resistivity, so the Hooge model is a good candidate for explaining the results. In any case, noise can be substantially reduced by increasing the volume of the bolometer.

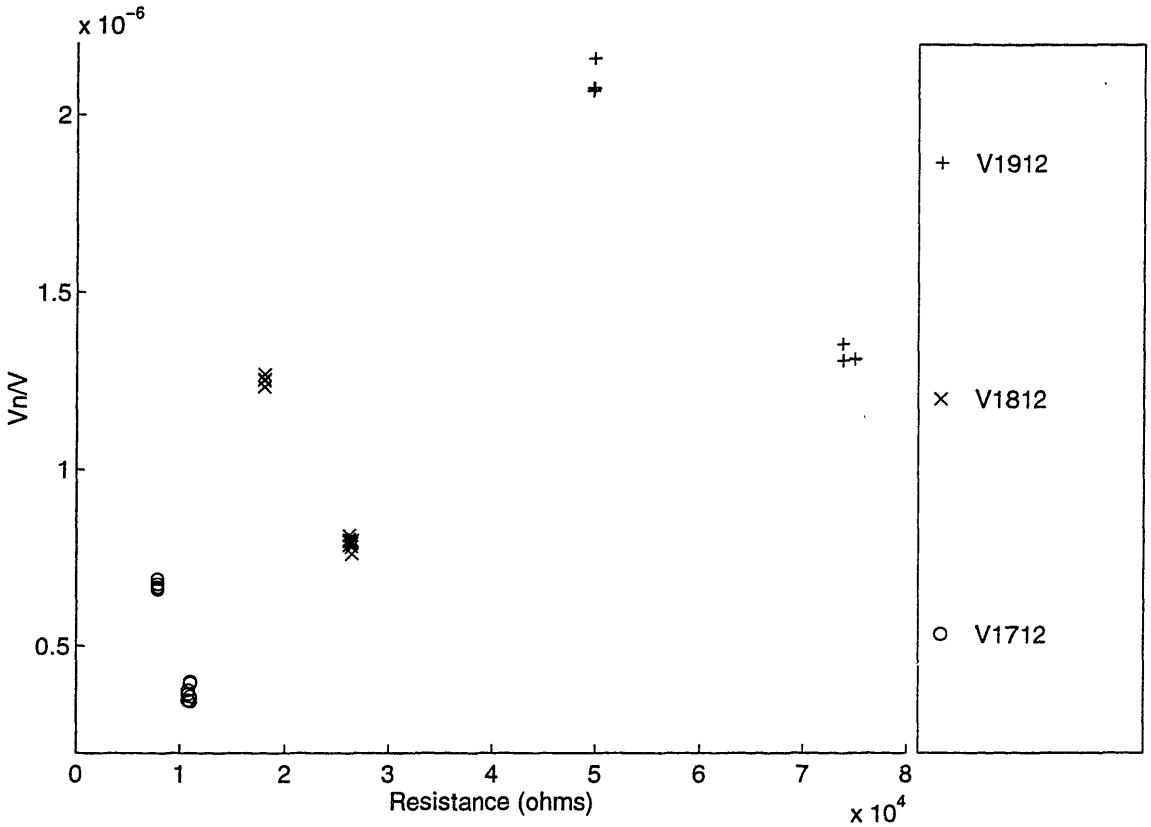

Figure 3-4: Thickness variation experiment

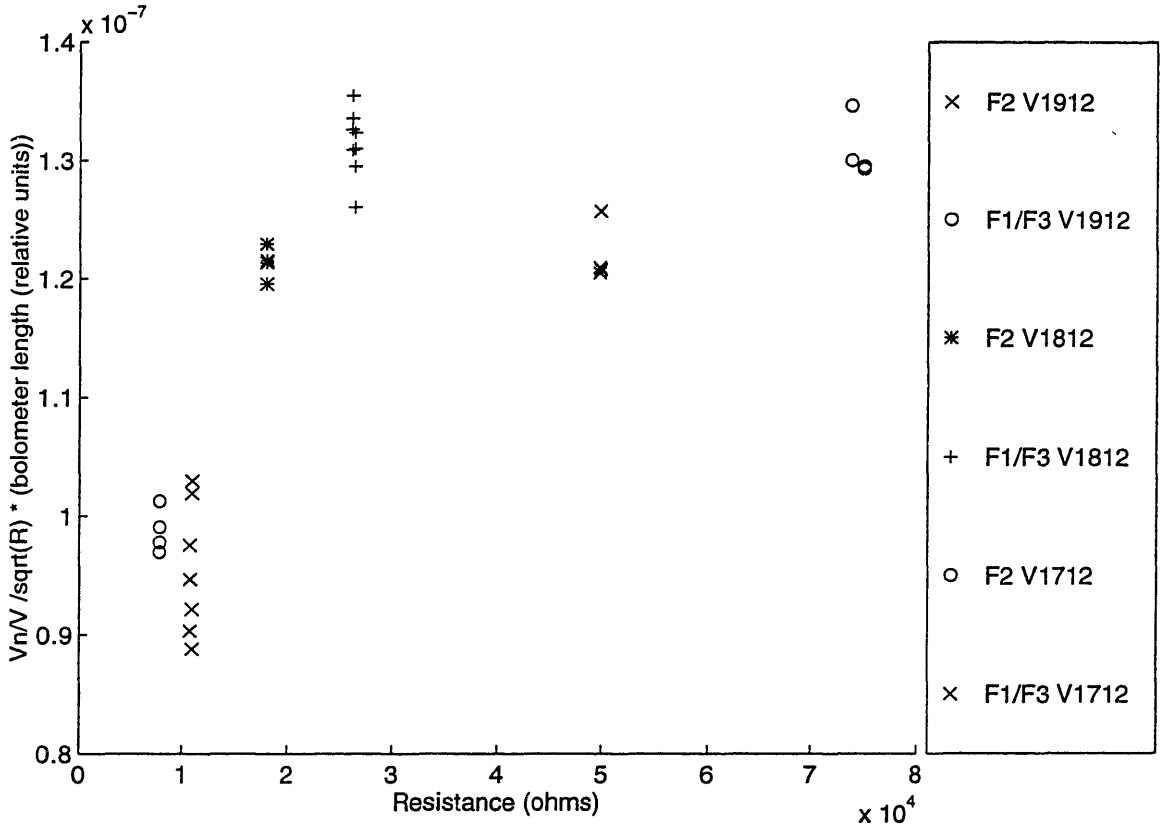

Figure 3-5: Bulk scaling on experimental parts

Chapter 4

System Noise Background

4.1 Introduction

In an ideal system, measurements would only be limited by fundamental detector noise. Any real system, however, contains some amount of extra noise. The noise of the investigated Uncooled system is broken down into two parts: detector noise, and read-out integrated circuit (ROIC) noise.

One needs a system model in order to analyze and evaluate noise actually viewed by users. A system noise model also allows one to determine what noise terms need to be measured. Once the required measurements are done, one can see how improving noise in various parts of the system affects the overall performance. Noise terms which particularly hurt overall performance can be identified and worked on first. In addition, a system noise model determines how much all the bolometer noise measurements from the previous part matter.

Models such as FLIR92 [3] already predict the performance of an IR system from basic noise and system parameters. Every system is unique however, so a model of the specific ROIC used is more useful than a generalized model.

4.2 Types of System Noise

Image noise can be separated into a few basic types. Spatial noise is usually defined as noise that does not vary much with time. Any fixed pattern appearing on the screen is spatial noise. Temporal noise is noise that depends strongly on time. It fluctuates a large amount from frame to frame.

Although the two groups above are useful in general descriptions of noise, finer characterization of noise is needed. The three main dimensions noise correlations exist in are rows, columns, and time. D'Agostino [3] gives a good overview of the three types of noise correlation and defines operators useful in separating the components from each other. Row noise is when there is a uniform variation along an entire row, but each row is different. Column noise is the same as row noise, but oriented vertically instead of horizontally. For simplicity, noise variations in time will be characterized as "white" for quickly fluctuating or "$1/f$" for slowly varying noise.

Any combination of the above three dimensions may exist, giving a total of 8 possibilities. For example, detector white noise is not correlated along rows or columns, so it is referred to as white noise. If an entire column fluctuates slowly, then the noise is $1/f$ column noise. If an entire row fluctuates rapidly, then it has white row noise. The causes of each type of correlated system noise are mainly left for future work, but a few ideas are presented later.

Not all noise terms are equally important to users of a system. Eye/brain averaging of scenes tends to pick up on noise which is correlated in time or space [6]. White noise tends to get averaged out, so it has a lesser importance. Common system figures of merit do not always take this into account. The FLIR92 model, when analyzing human perception of a noisy image, takes into account the eye/brain integration. The model can predict how well an observer will be able to make out fine details in an image. All observers are different, however, so there is some variation in the results. Even lighting conditions in the room during testing can affect how much noise is integrated out of an image [1].

4.3 System Figures of Merit

System figures of merit usually tend to be very dependent on the exact setup of the system. Lens size, refresh rate of the screen, and even lighting conditions can matter in a measurement. The two most widely used figures of merit for infrared systems are described below.

The minimum resolvable temperature difference (MRTD) is a purely human test of system performance. It is defined as the minimum temperature difference between a 4-bar target and background needed for a trained observer to resolve the image. Typically a person looks at the 4-bar target through the IR system being evaluated, and turns down the temperature difference between the target and its background until the target is no longer visible. The experiment is repeated several times. The measurement is a function of target size and orientation. For a trained observer, the measurement results are usually fairly repeatable. The MRTD measurement is a good test for real performance, since the effect of artifacts in the image such as row and column noise is always included.

A computable figure of merit more suitable for routine testing is the noise equivalent temperature difference (NETD). NETD is the temperature difference of a scene needed to give a unity signal to noise ratio. Sometimes it is divided into spatial and temporal components in an attempt to better model human preferences. Unfortunately it weights row and column noise the same as pixellated noise, so it may not lead to an accurate prediction of MRTD. From a user standpoint, MRTD is a better predictor of system performance. From a routine testing standpoint, NETD is faster and easier to measure.

4.4 ROIC Description

The read-out integrated circuit (ROIC) is a standard silicon-based circuit. The bolometer devices are grown directly over the ROIC. The ROIC measures the IR signal from each bolometer and sends the data off-chip in a digital format. Figure

4-1 shows the basic block diagram of the ROIC circuitry for a single bolometer pixel.

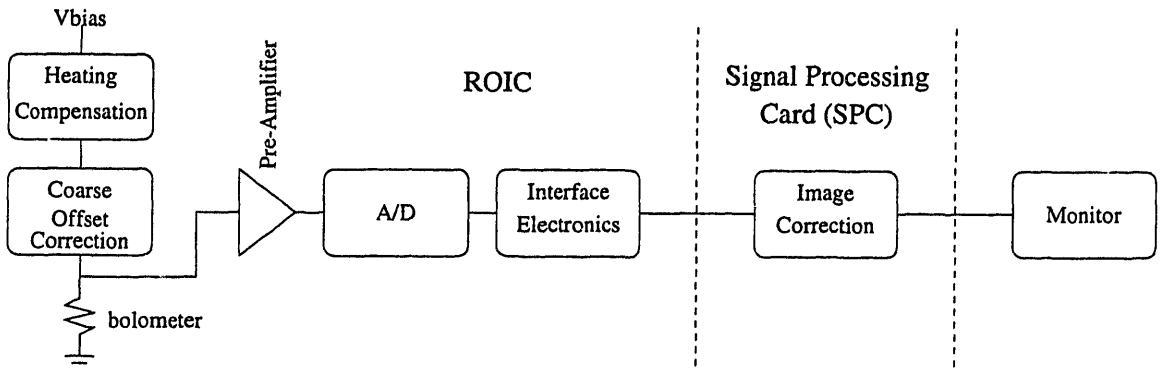

Figure 4-1: ROIC block diagram

The ROIC first biases each pixel to a voltage V_{bias} for a short period of time. Global heating compensation is done to correct for the bolometer change in resistance caused solely by bias heating (see the next section). A coarse offset, adjustable for each pixel, accounts for process variations in resistance. The offset, calculated on a uniform image, tunes the output of each bolometer to approximately the same value. By canceling out process variations, the dynamic range of the system is improved. Next, a pre-amplifier feeds the bolometer signal into an analog to digital (A/D) converter. Once in a digital format, the data is passed to the interface electronics and shipped off-chip to a signal processing board.

The circuitry in the ROIC is divided into rows and columns. The system scans down rows reading out about 320 values at a time. All detectors in a row are biased during the same period. All detectors in a column are read out by the same pre-amp and A/D circuitry. Noise correlations along a given direction can thus be traced to either the row or column circuitry.

The signal processing card, or SPC, provides fine offset and gain correction. Coarse correction on the ROIC only roughly cancels bolometer resistance variations. Fine offset correction on the SPC digitally corrects the image so it is uniform. A uniform black shutter (see Figure 4-2), controlled by the SPC, is used to get a uniform image for correction data. The SPC first records a frame looking at the shutter, then stores

whatever value is subtracted from each pixel value to get the output exactly in the middle of its range. A fine offset correction is done every few minutes to correct for slow drifts in pixel offsets.

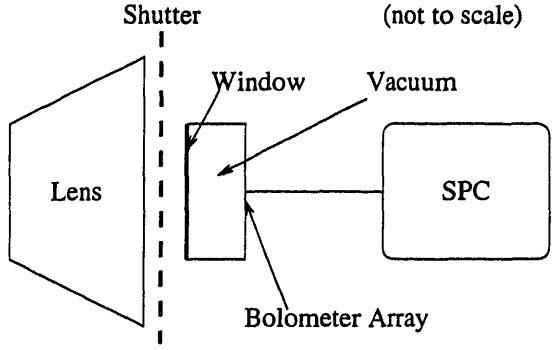

Figure 4-2: Lens and shutter location

Gain correction adjusts for differences in the gain of each pixel. The correction makes the scene look uniform for more than one temperature. The algorithm performs a two-point linear correction by measuring the response at two uniform scene temperatures. All pixels have a slightly different gain between the temperatures, so the output is digitally scaled.

In addition to simple gain and offset correction, the SPC also performs some non-linear gain processing to make the image easier to view. The signal coming from the ROIC is usually smaller than the dynamic range of the output. The basic idea is to fill the dynamic range for any picture so that the user can see a maximum amount of detail. The picture is analyzed with a histogram so that the hottest temperature in the scene does not show up as a dull grey, but as a bright white instead. Despite the visual enhancement, all gain processing was turned off during testing so that it did not complicate results.

4.5 Pulse Biasing

Bolometers burn out if the average power dissipated becomes too high. The goal of pulse biasing is to get an accurate measurement of bolometer resistance without using

too much power. The high refresh rate of 60 Hz requires a relatively fast measurement, also. Fortunately it turns out that keeping average power constant, it is possible to measure resistance with a given precision in any amount of time.

The basic idea behind pulse biasing is to take a sample every T_{sample} period of time, but only to bias for a fraction of the sampling period. The bias period, T_{bias}, is about $T_{sample}/240$ for the system under investigation. A total of about 240 pixel rows need to be read, but an entire frame is only read out every $1/60th$ of a second. Each row is biased sequentially for about $1/240th$ of the frame rate period.

To see why pulse biasing works, first consider the average power consumed by a bolometer biased for T_{bias} out of T_{sample} time. The average power is:

$$P_{avg} = \frac{T_{bias}}{T_{sample}} I^2 R \tag{4.1}$$

Assuming the current has a standard deviation of σ_I, integrating it for a time of T_{bias} results in a new standard deviation of $\sigma_I\sqrt{T_{bias}}$. The signal is the integrated current, or IT_{bias}. The signal to noise ratio (SNR) is thus given by:

$$\text{SNR} = \sigma_I\sqrt{T_{bias}} I \tag{4.2}$$

Plugging the signal to noise ratio into the average power equation, one finds that the average power reduces to:

$$P_{avg} = \frac{(\text{SNR})^2 R}{T_{sample}\sigma_I^2} \tag{4.3}$$

The average power is independent of T_{bias}, but does depend on the signal to noise ratio. More power means a better measurement, in general.

One problem that arises out of pulse biasing is that the instantaneous power is quite high, so the bolometer heats up a lot during the biasing period. One method of correcting for pulse biasing is to subtract off the extra current or voltage measured due to bias heating [4].

If no pulse bias heating correction is done, then the actual amount of temperature change due to pulse bias heating should be kept in check to avoid dynamic range

problems. Using a linearized temperature model [4], neglecting radiative loss, and biasing each bolometer directly, the temperature change over a pulse bias period T_{bias} is:

$$\Delta T = \frac{V^2}{RC} T_{bias} \left(1 + \frac{1 - \frac{V^2}{RC}(\mathrm{TCR}) T_{bias}}{e^{T_{sample}/\tau} - 1} \right) \tag{4.4}$$

where τ is the thermal time constant. The corresponding current change is $\Delta I = (\mathrm{TCR}) \Delta T \frac{V}{R}$.

4.6 System Model

In order to identify the most critical sources of noise, a system model incorporating all noise sources is necessary. In addition, a system model allows design changes to be quickly evaluated for their feasibility.

Thermal calculations on the bolometer give the responsivity and time constant of the device. The thermal conductivity, G, is completely determined by how much heat transfer occurs through the legs of the bolometer. Radiative loss is negligible in comparison. The 2 legs are made of metal and a covering material. The thermal conductance due to the metal of 2 legs is:

$$G_{metal} = g_{metal} w_{metal} \frac{t_{metal}}{l_{leg}} \cdot 2 \tag{4.5}$$

where g is the thermal conductance of the metal per μm, w_{metal} is the width of the metal, t_{metal} is its thickness, and l_{leg} is the leg length. The total conductance is just the sum of the metal and covering conductance, $G_{metal} + G_{covering}$.

The thermal capacity, C, is dominated by the bolometer itself, with a small contribution from the legs. For each material, one can look up the thermal capacity per unit weight, which is easily converted to c, the thermal capacity per unit volume. The bridge is composed of VOx and another covering material, so its thermal capacity is just $C_{bridge} = c_{VOx} V_{VOx} + c_{cover} V_{cover}$ where V is volume. The thermal capacity of the legs is estimated to be about half the volume of both legs. The total thermal capacity is just the sum of the bridge and leg contributions. The thermal time constant is then

defined as $\tau = C/G$.

Responsivity is defined as the change in output per degree change in the scene temperature. In this system, the output is in counts, a number ranging from 0 to 64000. To find responsivity, first calculate the change in resistance per degree change in the scene temperature:

$$\Delta R = \frac{\epsilon A I}{4F^2 + 1} \frac{\mathrm{TCR}}{G} R \tag{4.6}$$

where ϵ is the fill factor and absorption efficiency, A is the detector area in μm^2, I is the appropriate blackbody integral (discussed below) in Watts/μm^2/Kelvin, and F is the optics F number [2]. The detectors have a window over them which only allows radiation in the 8-14 μm range to pass through, so the appropriate blackbody integral is [5]:

$$I = \int_{8\mu m}^{14\mu m} \frac{dW_\lambda(T)}{dT} d\lambda \tag{4.7}$$

where $W_\lambda(T)$ is the spectral radiant emmitance of a blackbody at a temperature T.

The voltage for the A/D converter is obtained by first integrating the current onto a capacitor C_{int} for T_{bias} time, so the voltage change from a degree change in scene temperature is:

$$\Delta V = \frac{V_{bias} \Delta R T_{bias}}{R^2 C_{int}} \tag{4.8}$$

The responsivity is more conveniently expressed directly in the output units of counts. Volts are converted to counts by a scale factor determined by the A/D converter.

There are three main bandwidths when dealing with noise: electrical, thermal, and discrete-time/sampled. The thermal bandwidth is determined by the thermal time constant, and only affects the signal and thermal noise. The electrical bandwidth is for all the other noise terms, and is set by the integration time for each sample. The A/D converter integrates the current for a time of T_{bias} before sampling the result, thus effectively putting all noise and the signal through a low-pass filter. The discrete-time or sampled bandwidth needs to be considered because the images are only sampled at 60Hz, which is much lower than the electrical bandwidth. Substantial aliasing of noise does occur. The aliasing of Johnson noise does not hurt system performance, however, as seen in Section 4.5. When analyzing the results, one may only look at part

of the discrete-time bandwidth. Although this is more complicated than observing the entire discrete-time bandwidth, it is a useful condition for a model to handle.

The aliasing components of noise complicate the calculation of bandwidth for different power spectral densities (PSDs). The overall variance of noise passing through the integration stage and being sampled is given by:

$$\text{Variance} = \frac{1}{2\pi T_{bias}^2} \int_0^{\pi} \sum_{n=-\infty}^{\infty} S_{xx}(e^{j(\omega - n2\pi)}) \cdot 4 \left(\frac{sin((\omega - n2\pi)T_{bias}/2)}{(\omega - n2\pi)} \right)^2 d\omega \quad (4.9)$$

where ω is the frequency in radians and S_{xx} is the PSD of the noise. The signal also has a gain of T_{bias} during integration, so the variance is normalized by the gain squared, or T_{bias}^2. Care should be taken with factors of 2, since most references give PSDs (S_{xx}) in terms of a one-sided spectrum to avoid negative frequencies. Aliasing is generally easier to handle for 2-sided spectrums, though.

In most cases it is easier to think of the noise bandwidth before the signal is sampled. If one then looks at the entire discrete-time bandwidth, the variance does not change. For white noise, the effective electrical bandwidth is just $B_{electrical} = 1/(2T_{bias})$. For $1/f$ and thermal noise, Equation 4.9 should be used. An approximation that works fairly well for thermal and $1/f$ noise is to stop the sum over n when $n \approx 1/(2T_{bias}f_s)$ (where f_s is the sampling frequency), and approximate the *sinc* term as a constant T_{bias}. The approximation only works because the electrical bandwidth is much larger than the effective width of the thermal noise or $1/f$ noise.

Thermal noise is a random temperature fluctuation between the environment and the bolometer. It effectively acts as a low-pass filter with time constant τ, so its bandwidth from some low observed frequency f_l to a high observed frequency f_h is given by:

$$\begin{aligned} B_{thermal} \;=\; & \frac{1}{2\pi\tau} \sum_{n=1}^{N} [\arctan((nf_s - f_l)\tau) - \arctan((nf_s - f_h)\tau) \\ & + \arctan((nf_s + f_h)\tau) - \arctan((nf_s + f_l)\tau)] \\ & + (\arctan(f_h\tau) - \arctan(f_l\tau)) \end{aligned} \quad (4.10)$$

where N is approximately $1/(2T_{bias}f_s)$.

The thermal contribution to NETD is just:

$$\text{NETD}_{thermal} = \sqrt{4kT^2G}\sqrt{B_{thermal}}\frac{4F^2+1}{\epsilon AI} \tag{4.11}$$

where k is Boltzmann's constant and T is the ambient temperature. The thermal noise is well below the Johnson noise level for this system, so this term can usually be neglected. Thermal noise is the fundamental limit to bolometer performance when the bolometers have no $1/f$ noise.

Resistor Johnson noise is a significant contributor to system white noise. The effective bandwidth for white noise over the observed frequency range of f_l to f_h is:

$$B_{Johnson} = B_{electrical} \cdot \frac{f_h - f_l}{B_{system}} \tag{4.12}$$

where B_{system} is the Nyquist frequency (or half the sampling frequency). The Johnson noise contribution to NETD is thus given by:

$$\text{NETD}_{Johnson} = \frac{\sqrt{4kTR}}{V_{bias}}\frac{G}{\text{TCR}}\sqrt{B_{Johnson}}\frac{4F^2+1}{\epsilon AI} \tag{4.13}$$

$1/f$ noise from the bolometers has complicated aliasing characteristics, much like thermal noise. The effective $1/f$ noise bandwidth can be found using Equation 4.9 as:

$$B_{1/f} = \sum_{n=1}^{N}\left[\ln\left(\frac{nf_s - f_l}{nf_s - f_h}\right) + \ln\left(\frac{nf_s + f_h}{nf_s + f_l}\right)\right] + \ln\left(\frac{f_h}{f_l}\right) \tag{4.14}$$

From the previous chapter, $1/f$ noise can be modeled in two ways. It can either vary with the number of carriers, or with the volume; therefore, the noise figure of merit can be:

$$\frac{V_n}{V_{bias}} = \frac{\alpha}{\sqrt{V}} \quad \text{or} \quad \beta\sqrt{\frac{\rho}{V}} \tag{4.15}$$

where V is the VOx volume, ρ is the resistivity, α is the measured noise figure of merit normalized to volume, and β is the measured noise figure of merit normalized

to volume over resistivity. The $1/f$ NETD is thus given by:

$$\mathrm{NETD}_{1/f} = \frac{V_n}{V_{bias}} \frac{G}{\mathrm{TCR}} \sqrt{B_{1/f} \frac{4F^2+1}{\epsilon A I}} \tag{4.16}$$

Except for A/D white noise, the best way to get an accurate assessment of ROIC white and $1/f$ noise is to measure it. The A/D white noise for a perfect converter should be about $2\sqrt{1/12}$ counts.

If the measured white noise standard deviation is σ_w over the full electrical bandwidth, then the noise between f_l and f_h is approximately given by:

$$\sigma_w \sqrt{\frac{f_h - f_l}{B_{system}}} \tag{4.17}$$

If the measured $1/f$ noise in the full electrical bandwidth is $\sigma_{1/f}$, then the noise between f_l and f_h is:

$$\frac{\sigma_{1/f}}{\sqrt{\ln\left(B_{electrical}/f_l\right)}} \cdot B_{1/f} \tag{4.18}$$

Note that the f_l quantity must be larger than $1/T_{on}$, where T_{on} is how long the system has been on. There are 6 basic ROIC terms that need to be measured, which include: white row noise, $1/f$ row noise, white column noise, $1/f$ column noise, white noise, and $1/f$ noise. The overall screen fluctuation was ignored.

The total NETD of the system can be obtained by summing the individual NETD calculations in quadrature. In other words, the variance of the noise adds as:

$$\mathrm{NETD}_{total} = \sqrt{\sum_{x=\text{all noise terms}} \mathrm{NETD}_x^2} \tag{4.19}$$

4.7 System Model Checks

There are two main pieces of data which help verify the system model. The responsivity measurement plotted vs. resistance gives a good check on the optical and A/D characteristics of the system. Figure 4-3 shows that the system model predicts the general level and trend of the data for the normal bias voltage. The spread in the

data is most likely caused by variations in G, TCR, and responsivity measurement errors. Note that the model only has one value for parameters like G and TCR, while the actual measured parts each have a different value for those parameters. Figure 4-4 shows that the model also works well when the bias is 1.5 times higher than normal. Most of the responsivity model parameters are known approximately through measurements. A few, like ϵ (the bolometer fill factor), were adjusted slightly to get a better fit of the data.

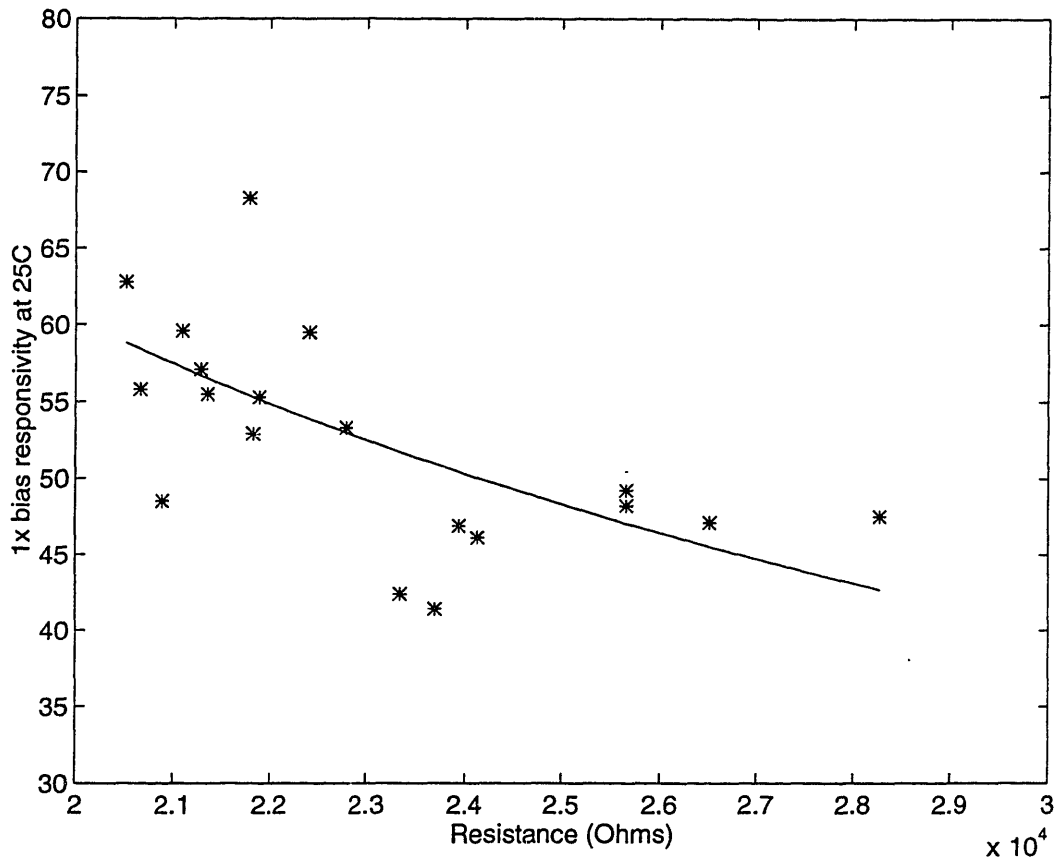

Figure 4-3: Responsivity modeling, normal bias

Another check on the model is to make sure it predicts the average measured NETD of the system. The data does correspond fairly well with the model, as seen in the next chapter.

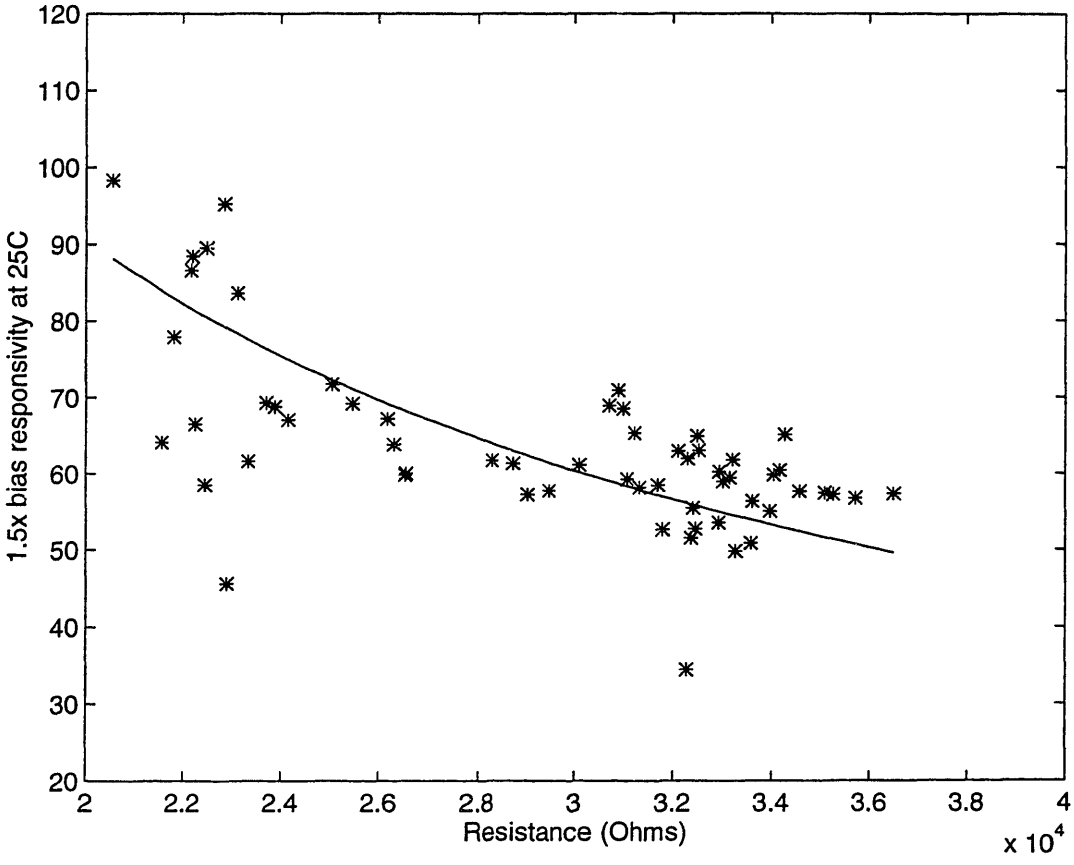

Figure 4-4: Responsivity modeling, 1.5x bias

Chapter 5

System Noise Tests

5.1 Overview

The main goal of system testing is to determine how much various components contribute to the overall noise. Parts of the system can be isolated by changing the software or hardware configuration of the system. The main parts characterized include the A/D, pre-amplifier, transistor switches, and bolometer noise. From these measurements, one obtains the required parameters for the system model.

In isolating the various parts of the system, one also needs to characterize the noise based on how it varies spatially and temporally. The spatial component of noise can be characterized as row, column, or pixel noise. Overall screen fluctuation is ignored. The temporal component of noise is broken down into $1/f$ and white noise.

5.2 Frequency Analysis

Characterizing noise on a single pixel seems relatively straightforward. In an ideal situation, one would take sequential frames and calculate a periodogram on the data for many pixels. The periodogram provides an estimate of the PSD without any knowledge of the underlying noise spectrum. Unfortunately, the investigated system is under development, so sequential frames of data were only available at roughly 20 second intervals. Since the camera sampling rate is at 60 Hz, grabbing a frame every

20 seconds does not yield useful results.

The signal processing card (SPC) provides a variable digital filter, however, which enables one to estimate spectrum parameters even without being able to take frames quickly. With enough data and a model of the PSD, one can extract a reasonable estimate of the noise parameters. One must assume something about the underlying spectrum, however, so the results are much less general than when directly doing a periodogram estimate.

The digital filter in the SPC is a recursive low-pass infinite impulse response filter. It has a single adjustable parameter, x; a lower x means a shorter filter and a lower passband on the filter. The algorithm for the low-pass filter basically keeps a running "average" of all past values to subtract from the current pixel value. In difference equation form, the average is:

$$g[n] = 2^{-x}x[n] + (1 - 2^{-x}) \cdot g[n-1] \tag{5.1}$$

where $x[n]$ is the value of a pixel at sample n, and $g[n]$ is the calculated average. The corresponding impulse response is $h_{avg}[n] = 2^{-x}a^n u[n]$, where $a = 1 - 2^{-x}$.

For each pixel, the output of the filter is actually the current pixel minus the previous average, or $x_{out}[n] = x[n] - g[n-1]$. The overall system impulse response is thus given by:

$$h_x[n] = \delta[n] - h_{avg}[n-1] \tag{5.2}$$

In order to see the effect of this filter on noise, one needs the magnitude of the filter frequency response squared as follows:

$$|H_x(f)|^2 = \frac{2 - 2\cos(2\pi T f)}{1 + a^2 - 2a\cos(2\pi T f)} \tag{5.3}$$

where T is the sampling period of the system. By varying x, $H_x(f)$ takes on a different shape which can be used to determine the parameters of the noise spectrum.

In order to determine the parameters of the noise spectrum, one must make some assumptions about its shape. A reasonable starting point is to assume that only $1/f$

and white noise are present. The spectrum is therefore modeled as $S_{xx}(f) = a^2 + b^2/f +$ aliasing terms. One way to separate $1/f$ and white noise involves calculating the effect of the filter on each noise variance separately. The total noise variance is approximately given by:

$$2T \int_{f_l}^{1/(2T)} S_{xx}(f)|H_x(f)|^2 df \tag{5.4}$$

where f_l is determined by the on time of the system and $f_l \ll 1/(2T)$. The white noise produces a mostly flat aliased spectrum at a height σ_w^2, so its variance coming out of the digital filter is $\sigma_{w,x}^2 = \sum \sigma_w^2 |h[n]|^2 = \sigma_w^2(1 + 1/(2^{x+1} - 1))$. The $1/f$ noise aliased spectrum is more complicated, so it is evaluated numerically for $b^2 = 1$ to give $\sigma_{1/f,x}^2$. The equation for the aliased $1/f$ noise spectrum is discussed in Chapter 4.

The basic procedure for finding the model parameters involves taking a frame at several different values of x (e.g., 0,2,4,6, and 8). Only one frame per x value needs to be taken assuming the noise is ergodic. Taking the standard deviation of one pixel in time is equivalent to taking the standard deviation of all the pixel values in an image. The set of linear equations resulting from the model is:

$$V\overline{x} = M \tag{5.5}$$

where

$$V = \begin{bmatrix} \sigma_{w,x=0}^2 & \sigma_{1/f,x=0}^2 \\ \sigma_{w,x=2}^2 & \sigma_{1/f,x=2}^2 \\ & \vdots \end{bmatrix} \quad , \quad \overline{x} = \begin{bmatrix} a^2 \\ b^2 \end{bmatrix} \quad , \quad M = \begin{bmatrix} \sigma_{m,x=0}^2 \\ \sigma_{m,x=2}^2 \\ \vdots \end{bmatrix} \tag{5.6}$$

where $\sigma_{m,x=n}^2$ is the measured noise variance at $x = n$. The least-squares solution is given by $\hat{x} = \left(V^T V\right)^{-1} V^T M$.

The results returned are for a^2 and b^2 without aliasing. When computing their contribution to overall noise at a given value of x, one must consider $V\hat{x}$. The data seems to fit the model fairly well. A typical plot of pixel noise containing both a $1/f$

and white noise component is shown in Figure 5-1.

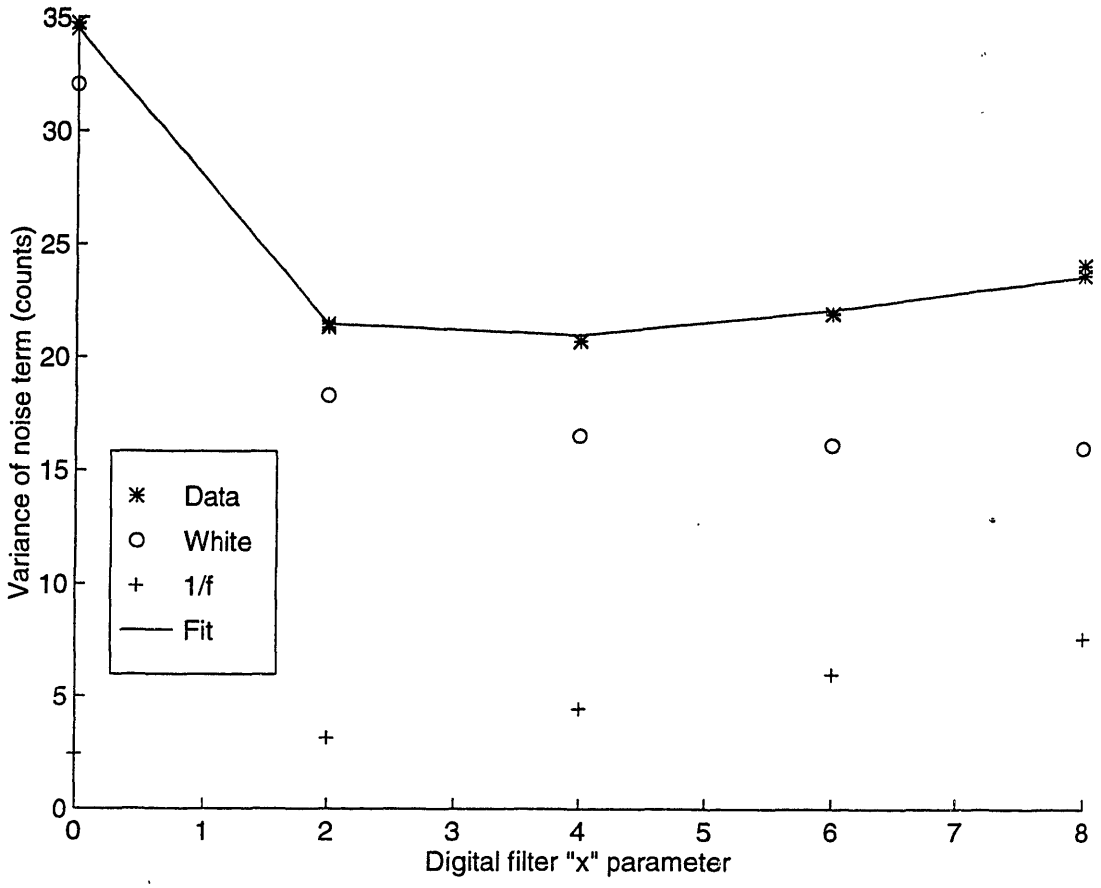

Figure 5-1: Noise variance vs. digital filter "x"

5.3 Spatial Separation

To identify whether noise is associated with individual pixels, row circuitry, or column circuitry, one must separate the noise based on its spatial correlation. For example, a uniform variation along an entire column is most likely caused by circuitry common to the entire column, such as the A/D or its buffer and pre-amp circuitry. The noise in an image is separated into row, column, and pixel components; all overall screen fluctuations are ignored.

The various types of noise are relatively straightforward to separate out. Taking

the average along each row, and then computing the variance of all the row averages gives the row noise variance. Column noise variance is found in the same fashion as row noise, except that the averages are across columns. Calculating the variance of the entire image after row and column averages have been subtracted gives the pixel noise variance. If pixel variance needs to be found when the detectors are enabled, then one should try and cancel out scene variations. Placing a piece of uniform black foam in front of the lens eliminates most scene variations. Putting the captured image through a high-pass filter helps get rid of the remaining scene variation due to the environment. The high-pass filter must be normalized to have unit energy so that the resulting overall variance is not changed.

5.4 Circuitry Separation

It is possible to electrically and physically disable parts of the ROIC to get a better idea of what parts cause the most noise. Disabling part of the circuitry is very useful in simplifying the analysis, but is also very time consuming.

The pre-amplifier and A/D circuitry noise show up when the detectors are disabled. In effect, one gets a good measure of overall ROIC noise by just disabling the detectors. The pre-amplifiers can be disabled separately from the A/D converters, allowing one to isolate any problems down to the pre-amplifier or A/D precisely.

Each detector gets selected by a MOS transistor switch which may have noise associated with it. One method of testing the switches for noise involves changing the gate voltage on all the transistors. Changing the gate voltage should result in some change in the noise.

A good check to see if detector noise is measured correctly is to examine its dependence on the bias voltage across each bolometer. White noise and $1/f$ noise both depend differently on bias. The NETD due to white noise (in counts per mK) goes down as bias is increased, while $1/f$ NETD stays the same.

5.5 A/D Testing

Disabling the detectors and pre-amplifiers gives a clean measurement of A/D noise. Unfortunately, disabling circuitry on a board is time-consuming and sometimes risky to the product. A faster and easier way of testing for A/D noise involves changing the integration time of the detector current. The detectors are still biased for the same amount of time, but the current is only integrated for some fraction of the bias time. The integration time is changeable entirely with software commands.

The A/D noise is constant no matter what the integration time, while the noise before the A/D goes up as a function of integration time. Because integrating the current acts as a low-pass filter, $1/f$ noise and white noise react differently to a change in integration time. For white noise, the voltage noise variance on the input to the A/D converter is:

$$V_{n,white}^2 = 4kTRBg^2 \tag{5.7}$$

where $B = 1/(2T_{int})$ is the white noise bandwidth and $g \propto T_{int}/(RC)$ is the gain on the detector signal. The noise variance of white noise thus varies as $V_{n,white}^2 \propto T_{int}$. With $1/f$ noise, the total noise changes insignificantly when the integration time is increased because more aliasing has virtually no effect. The voltage noise variance is therefore proportional to g^2, or $V_{n,1/f}^2 \propto T_{int}^2$. Given the above differences in white noise, A/D noise, and $1/f$ noise, it is possible to separate all three components. If possible, it is better to eliminate variables from the model. For example, if $1/f$ noise is known to be insignificant, then including it in the integration time analysis only leads to greater error. The frequency separation analysis should be done before attempting to separate A/D noise, otherwise much more data needs to be taken to ensure accurate results. Unfortunately separating the overall noise into white noise and $1/f$ noise first introduces error even before the two types of noise can be separated into A/D and non-A/D noise. In other words, the estimates of $1/f$ noise and white noise each have a greater percentage error than a single estimate of the total noise.

To find the A/D noise, frames should be taken at various values of integration time. The model for the noise as a function of integration time is $\sigma^2 = \sigma_{A/D}^2 +$

$T_{int}\sigma_w^2 + T_{int}^2\sigma_{1/f}^2$, where σ_{noise}^2 is the noise variance due to A/D, $1/f$, or white noise. When data is taken at many integration times, the resulting set of linear equations is:

$$T\overline{x} = V \tag{5.8}$$

where

$$T = \begin{bmatrix} 1 & T_{int,1} & T_{int,1}^2 \\ & \vdots & \\ 1 & T_{int,N} & T_{int,N}^2 \end{bmatrix} \quad , \quad \overline{x} = \begin{bmatrix} \sigma_{A/D}^2 \\ \sigma_w^2 \\ \sigma_{1/f}^2 \end{bmatrix} \quad , \quad V = \begin{bmatrix} \sigma_{Tint,0}^2 \\ \vdots \\ \sigma_{Tint,N}^2 \end{bmatrix} \tag{5.9}$$

where $\sigma_{Tint,n}$ is the measured variance at an integration time n.

The results in Figure 5-2 show that $1/f$ noise variance does vary approximately as T_{int}^2 and white noise varies as T_{int}.

5.6 Experimental Results

Preliminary testing on a few focal planes suggest that there are only 5 main noise terms: white row noise, $1/f$ column noise, A/D white noise, bolometer white noise, and bolometer $1/f$ noise. All other noise sources give a negligible contribution to overall noise. Table 5.1 summarizes the data taken on several focal planes. All data variances are given for the digital filter parameter $x = 6$.

The test conditions summarize what changes were made to each focal plane before testing. For example, "1.5x bias" specifies that the bias voltage across the detectors was 50% higher than normal, "1.5x switches" specifies that the voltage on the transistor switches was 50% higher than normal, and "preamp x4" means the pre-amplifier current was 4 times higher than normal.

The data, as seen in Table 5.1, is somewhat noisy. The main reason for the variation in results is because only a small number of points were taken at each value of x and T_{int}. No rigorous analysis of the error on any extracted parameter was done. In addition, some focal planes had a small number of very noisy pixels which

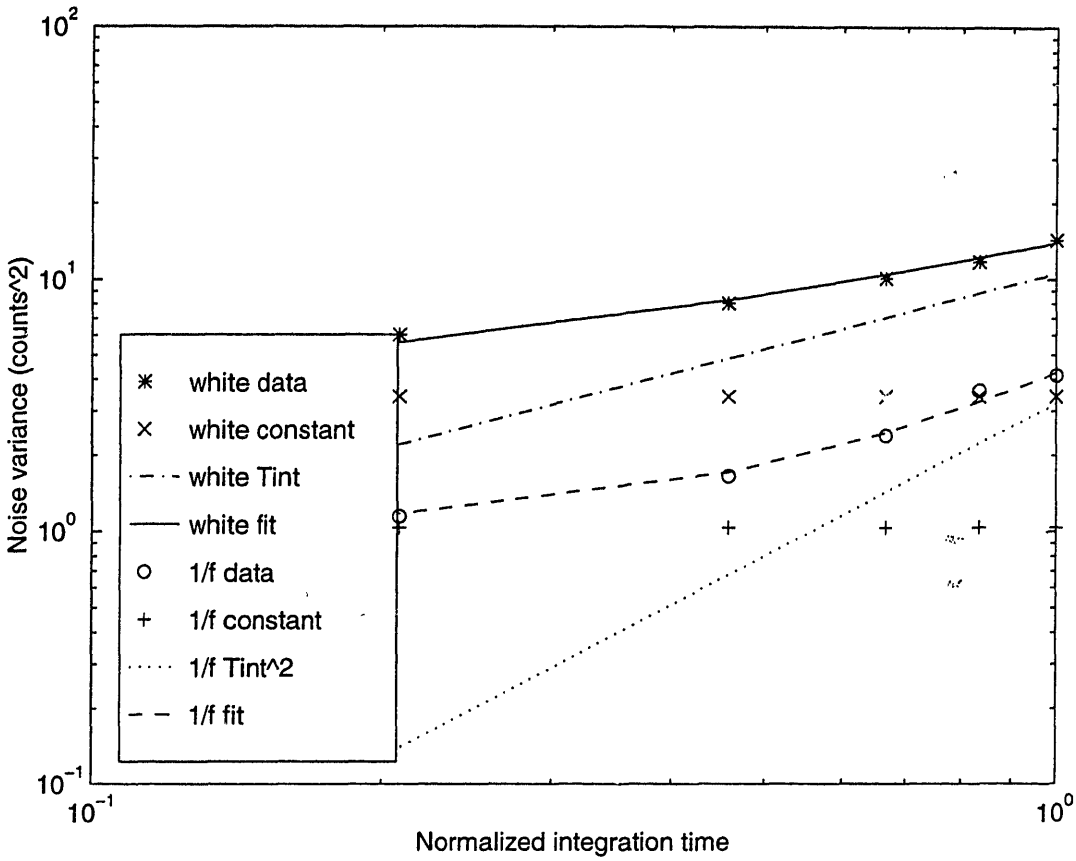

Figure 5-2: Noise variance vs. normalized integration time

introduced even more error into results. Responsivity measurements used to convert from counts to mK also seem to only be repeatable to within roughly ±5-10%. To achieve better results, more data points with better focal planes should be tested.

Despite the shortcomings of the data accuracy, it does show the basic trends expected in the data. With increasing bias, the NETD due to pixel white noise drops. The pixel white NETD does not drop as quickly as predicted by Equation 4.13, however. It is not known whether the problem is in the fitting algorithm, whether more noise is introduced at higher biases, or whether some other small white noise term is present. The $1/f$ NETD stays about the same, as predicted. The integration time analysis agrees well with data taken with just the A/D enabled. The approximate $1/f$ and white noise levels also agree well with the system model

FPA	Test Conditions	White Row Noise (counts)	$1/f$ Column Noise (counts)	A/D White Noise (counts)	Pixel White Noise (counts, mK)	Pixel $1/f$ Noise (counts, mK)
188	1x bias	1.8	0.8	2.2	2.4 , 60	1.8 , 45
	1.5x bias	1.8	1	2.2	2.8 , 47	2.8 , 43
	1.5x bias, 1.5x switch	1.8	1	assumed 2.2	2.8 , 4.7	2.8 , 43
	A/D and preamp x1	1.8	0.8	2.2		
	A/D and preamp x4	1.6	0.8	2.6		
	A/D only	1.4	0.8	2.2		
263	1.5x bias	1	0.6	2.2	2.8 , 45	2.4 , 38
293	1.5x bias	1	0.6	2.4	2.2 , 65	1.6 , 48
294	1x bias	1.6	0.34	2.4	2.2 , 60	1.8 , 49
	1.5x bias	2.2	0.22	2	2.8 , 51	2.4 , 44
	1x bias, 1.5x switch	1.6	0.28	2.4	2.2 , 60	1.8 , 48
	A/D only	1.6	0.22	2.2		
372	1.5x bias	0.8	0.6	2.6	2.8 , 64	1.8 , 43
406	1.5x bias	1	0.6	2	3.2 , 62	2.0 , 40
408	1.5x bias	1.4	1	2	2.4 , 49	2.8 , 39

Table 5.1: ROIC testing summary

developed in Chapter 4. The modeled white noise NETD (in mK) at normal (1x) bias is about 50 mK, while the experimental results give a white noise around 60 mK. The modeled $1/f$ noise ranges from about 30 mK to 50 mK, white the data in Table 5.1 ranges from 39-49 mK. The predicted bolometer $1/f$ noise varies over such a large range because the noise figure of merit, V_n/V_{bias} varies also. With such a wide range of predicted values, it is difficult to tell exactly how much error the modeled $1/f$ noise has. The model has many unknown parameters which were estimated, so it only serves to give a rough estimate of the actual noise observed in the system.

5.7 Discussion

The measurements on various ROICs show that $1/f$ noise from the bolometers themselves dominate the low-frequency noise characteristics of the system. The final column in Table 5.1 is completely determined by bolometer characteristics. Since MRTD measurements are mainly influenced by low-frequency noise that the eye does not tend to integrate out, reducing low-frequency noise is a high priority. Column $1/f$ noise also significantly affects an image because of its spatial correlation, even though its magnitude is much less than the bolometer $1/f$ noise. The cause of the column $1/f$ noise was identified before this noise study began, however, and can be fixed by a small change to the ROIC circuitry.

The three white noise components are all very roughly equal in magnitude. The row white noise is most visible in an image because of its high spatial correlation. The cause of the row noise is not certain, but several sources were identified separately from this thesis and are being corrected.

The A/D white noise has a magnitude much higher than expected. As discussed previously, the expected theoretical noise is only about $2/\sqrt{12} \approx 0.6$ counts, while the actual A/D noise of about 2.2 counts is much higher. A brief investigation into the A/D noise uncovered that some of the noise is due to crosstalk with the chip output drivers. The fact that the A/D noise varies with a period exactly equal to the rate the output drivers ship data off the chip strongly suggests a connection between the two. Further investigation needs to be done in order to reduce A/D white noise and determine if crosstalk is the only cause of the excess noise.

The pixel white noise magnitude is roughly equal to the predicted bolometer white noise. The bolometer white noise is a fundamental noise term which can be reduced in many ways. Increasing the bias on each bolometer reduces the effect of Johnson white noise. The Johnson white noise does not actually change as bias increases, but the signal increases (see Equation 2.2), so the signal to noise ratio goes up. $1/f$ noise, however, increases with bias at the same rate the signal does, so changing the bias does not affect the signal to $1/f$ noise ratio.

The overall system performance from a user standpoint would benefit most by reducing the bolometer $1/f$ noise, row white noise, and column $1/f$ noise. Bolometer $1/f$ noise can be reduced by increasing the volume of VOx, as discussed in Chapter 3. Column $1/f$ noise should no longer be a problem as the next ROIC chip is fabricated. Row white noise was separately investigated and several fixes will be tested.

Chapter 6

Conclusion

The main goal of this thesis was to identify the major sources of noise in an Uncooled system and try to reduce them, especially if the noise originated with the bolometers themselves. Chapter 2 dealt with an extensive testing and verification strategy on the bolometer devices. The experimental results confirmed that the data is repeatable and valid; the measured noise actually comes from the bolometers and not some external source. Chapter 3 described with the results of testing many bolometers and some new experiments which ensued. The noise of a bolometer may be substantially lowered by increasing its volume. Resistivity affects $1/f$ noise, but further tests are needed to determine if the observed noise fits the Hooge model. Chapter 4 developed the necessary framework for interpreting system noise measurements. A simple model which roughly fit measured system parameters was developed. Chapter 5 presented the experimental results obtained on several Uncooled focal planes. The major sources of noise that influence image quality were identified as bolometer $1/f$ noise, column $1/f$ noise, and row white noise. All three noise terms can be reduced, either through VOx material changes or ROIC circuit modifications.

Bibliography

[1] L. Biberman. *Perception of Displayed Information.* Plenum Press, New York, 1973.

[2] N. Butler, R. Blackwell, R. Murphy, R. Silva, and C. Marshall. Low cost uncooled microbolometer imaging system for dual use. In *SPIE*, number 2552, pages 583–591, 1995.

[3] John A. D'Agostino. Three-dimensional analysis framework and measurement methodology for imaging system noise. *Proceedings of the IRIS Passive Sensors Symposium*, 1991.

[4] Christer Jansson, Ulf Ringh, and Kevin Liddiard. Theoretical analysis of pulse bias heating of resistance bolometer infrared detectors and effectiveness of bias compensation. In *SPIE*, number 2552, pages 644–652, 1995.

[5] R.H. Kingston. *Detection of Optical and Infrared Radiation.* Springer Series in Optical Sciences. Springer-Verlag, New York, 1978.

[6] J.M. Lloyd. *Thermal Imaging Systems.* Optical Physics and Engineering. Plenum Press, New York, 1975.

[7] James H. McClellan, C. Sidney Burrus, Alan V. Oppenheim, Thomas W. Parks, Ronald W. Schafer, and Hans W. Schuessler. *Computer-Based Exercises for Signal Processing using Matlab 5.* Matlab Curriculum Series. Prentice-Hall, Upper Saddle River, New Jersey, 1998.

[8] C.D. Motchenbacher and J.A. Connelly. *Low-Noise Electronic System Design.* J. Wiley and Sons, New York, 1993.

[9] Richard F. Voss and John Clarke. Flicker $(1/f)$ noise: Equilibrium and resistance fluctuations. *Physical Review B*, 13(2):556–573, 1976.

[10] William L. Wolfe and George J. Zissis, editors. *The Infrared Handbook.* Environmental Research Institute of Michigan, Ann Arbor, Michigan, 1985.

[11] A. Van Der Ziel. Flicker noise in electronic devices. *Advances in Electronics and Electron Physics*, 49:225–297, 1979.

THESIS PROCESSING SLIP

FIXED FIELD: ill. _____ name _____

index _____ biblio _____

► COPIES: (Archives) Aero Dewey (Eng) Hum

Lindgren Music Rotch Science

TITLE VARIES: ► ☐ _____

NAME VARIES: ► ☐ _____

IMPRINT: (COPYRIGHT) _____

► COLLATION: 82 p.

► ADD: DEGREE: _____ ► DEPT.: _____

SUPERVISORS: _____

NOTES:

cat'r: date:

page:

► DEPT: E.E. ► J142

► YEAR: 1998 ► DEGREE: M. Eng.

► NAME: LENTZ, William Alexander